UNIVERSITY OF SOUTHAMPTON

DEPARTMENT OF SHIP SCIENCE

FACULTY OF ENGINEERING AND APPLIED SCIENCE

Computational Fluid Dynamic Investigation of Hull-Waterjet Flow Interaction.

By
A.W.Hughes & S.R.Turnock

Ship Science Report No.102
September 1997.

COMPUTATIONAL FLUID DYNAMIC INVESTIGATION OF HULL-WATERJET FLOW INTERACTION

By

A.W.Hughes & S.R.Turnock

Department of Ship Science
University of Southampton

Ship Science Report No.102

September 1997.

COMPUTATIONAL FLUID DYNAMIC INVESTIGATION OF HULL-WATERJET FLOW INTERACTION

A.W.Hughes & S.R.Turnock
Department of Ship Science.
Report No.102
September 1997.

ABSTRACT

A comparison of reliable experimental data with the prediction of a Computational Fluid Dynamics (CFD) package for the flow over and through the upstream hull and inlet duct of a water-jet geometry has been carried out. The flow solver algorithm used is based on the incompressible, three-dimensional Reynolds averaged Navier-Stokes equations for turbulent flow with a k-ε turbulence model. A detailed series of wind tunnel tests of a representative water-jet geometry have been carried out for a range of duct exit velocity to ship speed ratios. Detailed surface pressure measurements and velocity profiles within the duct were obtained. A multi-block grid generator was used to produce a computational mesh of the water-jet inlet duct and wind tunnel working section which represented the ship hull. Solutions were obtained for comparable conditions to those tested. It was found that both the surface pressure variations and velocity profiles along and around the duct were well predicted as was the influence of operating condition. The differences found were principally attributed to the lack of grid resolution for the boundary layers and in areas of rapidly changing curvature. The CFD working section was then changed for a flat plate surrounding the duct inlet. This model was used to study the influence of pitch and yaw on the pressure distributions along the duct and velocities at the impeller face plane. The results were promising and the predicted trends were as expected. In addition, modelling the influence of a simple hull shape on the flow through the water-jet inlet has been investigated. The ability of the flow solver to obtain reasonably accurate solutions was demonstrated, allowing predictions to be made of the total force distribution on both the hull surface in the vicinity of the duct and on the inlet duct itself. It is concluded that it is possible to model the water-jet system at present and obtain practical design information. However, significant improvements are still required to the methods by which complex three-dimensional shapes are defined in order to allow rapid parametric studies.

TABLE OF CONTENTS

LIST OF FIGURES

LIST OF TABLES (Appendix C)

NOMENCLATURE

Cp	Non-dimensionalised pressure coefficient.
g	Acceleration due to gravity (m/s^2).
H	Height of water in Betz manometer (m).
$\dot{m}$	Mass flow rate (kg/s).
P	Pressure (N/m^2).
R	Resistance (N).
T	Thrust (N).
t	Thrust deduction factor.
U	Air velocity (m/s).
Ve	Water-jet duct exit velocity (m/s).
Vi	Water-jet duct inlet velocity (m/s).
ρ_a	Density of air (kg/m^3).
ρ_w	Density of water (kg/m^3).

1. INTRODUCTION

The water-jet provides an efficient means of propulsion in a speed range of direct relevance to fast craft. Although the concept of jet propulsion has been around for many centuries, it is only in recent decades that advances in propulsion technology have enabled systems to be fitted on large scale vessels. However, the application of water-jets to commercial fast craft is still relatively new. As a result there are a number of key areas where the ability to understand more fully the complex nature of the fluid flow through the water-jet, and the interaction of the whole unit with the surrounding structure, would enable further improvements in performance to be made and lead to a more effective design of hull-water-jet systems.

The quality of the onset flow into a water-jet inlet can strongly influence impeller pump performance. Additionally, at the preliminary design stage the influence on hull thrust deduction due to the water-jet inflow still has a high level of uncertainty associated with it. Recent advances in Computational Fluid Dynamic (CFD) flow solvers offer the ability to model the flow over the hull and through the water-jet inlet. Advantages of CFD analysis include the ability to carry out a range of parametric tests without the need to re-use expensive test facilities. However, the complex shape of the water-jet duct and its surrounding hull present difficulties to current CFD codes. Further problems occur when necessary extra details such as the drive shaft, inlet grills and lip shapes are included in the model geometry. Before these details can be considered, it is required to have confidence in the validity of the three-dimensional flow solution obtained through the basic duct alone. For this to be done, it is necessary to obtain detailed and accurate experimental data of the flow for comparison purposes.

Increasing popularity in the use of water-jets as a propulsive device has seen a rise in the amount of research being conducted on them. The main body of the work has been to determine the characteristic behaviour of such units in an attempt to increase their efficiency and to understand interaction effects with the surrounding hull. Work has involved both experimental and computational analysis.

Okamoto et al[1] used a towing tank to investigate the pressure distribution on the inner surface of a water-jet duct in self-propulsion conditions. Their results indicated additional thrust generation on the intake duct. However, it was stressed that the complete evaluation of the force acting on the intake duct required the introduction of a viscous CFD code. Two-dimensional diffuser and lip section shape were investigated by Pylkkanen[2]. Later using a CFD flow solver Pylkkanen[3] modelled a flush-type intake duct with a two-dimensional mesh which represented the centre-line plane of the duct. However, Dai et al[4] considered that the geometry used by Pylkkanen was too restrictive for the investigation of these complex three-dimensional flows.

Experimental methods which have been used for the testing of water-jets have been successful, however, they are expensive and time consuming. It is for this reason that more research is being carried out with the use of CFD, and as the computer technology advances, results are becoming more accurate. However, experimental results are still required in order to validate the CFD predictions. The majority of papers reviewing CFD research have compared their results with existing test data. On the whole, the comparisons have been good, however, some discrepancies have also come to light.

One significant reason for these disagreements is that the CFD model geometries differ from the physical model or the full scale unit upon which they are based. This is due to the limitations of the computational codes. The most difficult objects to model through a water-jet are its internal appendages; the intake grill, drive shaft and impeller. Due to the complexity of these problems they have usually been excluded from the water-jet geometry which has remained a relatively simple intake duct. In order to obtain a suitable validation of a CFD code requires the experimental geometry to be of the same shape and size. Many of the computational models have also been run flat with an inlet flow parallel to the duct centre-line, this is unlikely to be the case in reality. Very little published work has examined water-jet ducts operating in off-design flows.

The Department of Ship Science has carried out a programme of work on water-jet hydrodynamics over the last three years. The major component has been the development and testing of a wind tunnel scale model of a representative water-jet inlet duct. Moss[5] constructed the model for the wind tunnel and recorded surface pressure measurements and velocity profiles along the duct during several operating conditions. His aim was to assess the feasibility of modelling water-jet intake units using air rather than water and to investigate pressure distributions within the duct. The model was produced reasonable results and the potential of wind tunnel testing of water-jets was shown. The model's impeller was further developed by Pease[6] allowing more flexibility with the flow conditions through the duct.

Theoretical studies have also been carried out. English[7] modelled the same duct using a lifting surface panel method which was initially developed to model the interaction between ship propeller and rudder. A source was used to represent the impeller pulling the flow through the jet however, the method did not take into account that the flow at a water-jet impeller varies spatially and temporally. The lifting surface formulation was also irrotational and inviscid and there was therefore a lack of boundary layer and subsequent areas of cavitation and separation had to be estimated.

Hughes[8] created a basic computational model of the duct geometry which he and Moss[5] had used for wind tunnel experiments. A commercially available CFD code was used to create a three-dimensional multi-block mesh of the duct. In order to recreate the experimental test set-up the wind tunnel working section was also modelled. The results obtained were compared with those from the experiments. It was seen there was some concurrence with the experimental results, however, the computer geometry of the duct was simplified in order for it to work, thus altering the flow through the duct slightly. For this reason a thorough comparison could not be made.

The aim of the work presented in this report has been to develop a three-dimensional Reynolds averaged Navier Stokes (RANS) computational model of a water-jet inlet duct and upstream hull which includes the effects of viscous, rotational flow and which is validated through comparison with detailed surface pressure and velocity data. The report begins by giving a brief description of the history and principles of water-jet propulsion. A model of a representative water-jet duct was studied using a wind tunnel and the report discusses in some detail the experimental set-up, procedure and results. The wind tunnel test results are then used to validate predictions made by a commercial CFD flow solver for this water-jet geometry. The complete generation of the CFD

model is described; the duct geometry definition, solution strategy, results obtained and the validity of the results. The report then expands this initial CFD geometry into a model which includes the aft half of a hull surrounding the duct. Stages along the way include investigations into the effects of pitch and yaw on the flow through, and the forces acting on the duct. Interaction effects are discussed briefly before a summary of the work is given, conclusions drawn and recommendations made for further work.

2. WATER-JETS

2.1 HISTORY [9]

Water-jets are not a new idea. As early as the 1630's, at a time when there was much interest in using steam to raise water, David Romsey acquired a patent which included an invention to propel vessels "...against Stronge Winde and Tyde." However, early proposed water-jet devices were not able to compete with paddle wheels and, later, propellers because of the limited technology and lack of understanding of the theory of propulsion.

By the 1950's pumps had improved in efficiency and were used successfully in marine vehicles for this purpose. Since the mid-1970's water-jets have grown in popularity and now provide a useful means of propulsion for many applications, from small one-man jet skis to large passenger ferries.

Water-jet inlets can be divided into two main categories; pod inlets and flush inlets. Pod inlets, sometimes called ram inlets, are generally used for more specialised applications such as hydrofoils and vessels where air ingestion may occur regularly. Flush inlets are far more common and tend to be used on all other craft including conventional monohulls, planing craft, catamarans and surface effect ships.

2.2 OPERATING PRINCIPLE

The basic operating principle of water-jet propulsion is similar to that of a screw propeller system. The propelling force is generated by adding momentum to the water by accelerating a flow of water in an astern direction. Water from beneath the vessel's hull is fed through an inlet duct to a pump which adds head to the water. This head is then applied to increase the velocity, hence momentum, when the water passes through an outlet nozzle usually mounted on the transom. The normal head of water in the duct varies at different speeds and careful design of the shape - ranging from an elliptical form on the hull bottom to a circle on the transom (for a flush intake) - is necessary to avoid 'choking' and to ensure a regular flow with minimal losses.

Typical components making up a marine water-jet are illustrated in Fig.1, they include an intake duct, a pump element, a nozzle and a steering/reversing mechanism. Steering and reversing forces are generated by deflecting the jet with a bucket gear which is normally operated by hydraulics. Achieving the best efficiency requires the tuning of all these components to the working conditions of the specific application.

2.3 THE REPRESENTATIVE WATER-JET DUCT

The water-jet duct being considered is a flush inlet and the general form (Fig.2) follows that used by Okamoto et al[1] for their model self propulsion tests. It was chosen to allow comparison with their experimental data. However, a few minor alterations were made to ease construction of a scale model which was built for wind tunnel testing. The inclination of the duct centre-line is 25 degrees and the lower half of the duct is semi-circular. The front-end of the upper half is rectangular in cross-section which changes gradually into a half circle. The flat upper surface allowed a model to be constructed partially of perspex to ease flow visualisation, it also facilitated the use of a simpler clamping and traverse device for holding pitot probes. The numerical model was based on the wind tunnel model dimensions and shape.

3. WIND TUNNEL TESTS

3.1 AIMS

A data base of reliable and accurate measurements of the flow through a representative water-jet duct was required for validating calculations by a CFD flow solver. Wind tunnel tests were decided upon as a means of modelling the duct. A wind tunnel allowed a more effective testing environment than either towing tank or cavitation tunnel facilities. The duct and all the necessary apparatus remained fixed in one position whilst the fluid was drawn past the duct. Each run could take as long as required. The duct would be investigated using surface pressure tappings around the duct walls, leading to pressure coefficient (Cp) distributions, and traverse probing of the flow using pitot probes in order to obtain velocity profiles.

3.2 EXPERIMENTAL SET-UP

The shape of the scale model, Fig.2, was similar to that used by Okamoto et al[1]. The diameter of the water-jet outflow was 0.254m compared to the 65mm used by Okamoto. The model was built from faired thin strips of 1.5mm plywood attached to a base plate by a series of ribs which defined the outline shape. The front face of the unit was transparent and this allowed detailed flow visualisation using wool tufts taped to the inside of the duct. The base plate was designed to fit exactly into the side of the working section of a 0.9m x 0.6m open circuit wind tunnel. Attaching the duct to the side of the wind tunnel meant the duct is actually tested in a horizontal position rather than vertically, as it would operate in reality. However, as the fluid used was air rather than water, gravitational effects could be assumed as negligible. A total of eighty five static pressure tappings were fitted to the wall of one half of the jet unit, along a number of radial and longitudinal sections. In addition, eight ports were located along the top wall of the model allowing pitot probes to be traversed through the duct.

Air was drawn through the wind tunnel by a fan situated at the end. The use of an open (non-return) wind tunnel results in the pressure within the working section of the tunnel being below atmospheric pressure. A variable speed 30KW impeller was installed aft of the jet unit in order to overcome the negative pressure within the working section and to allow the flow rate through the duct to be controlled. Due to restrictions in the space available, the impeller had to be connected to the jet unit via a flexible tube of similar diameter to the duct exit. Fig.3 illustrates the experimental rig set-up.

3.3 DATA ACQUISITION

The large number of individual data readings required the use of an automated system for data acquisition. The pressure tappings around the duct wall were connected via a rotary 1 p.s.i. scanivalve to an automated system which converted pressures into voltages. These voltages could then be read by a voltmeter connected to a PC which collected and stored the data. The reference pressure used P_A was taken at the top centre-line port at outflow plane (A: x=-0.3) of the water-jet and non-dimensionalised using the total head P_T measured at the centre of the outflow relative to the wall static P_A. The non-dimensionalised pressure coefficients (Cp) were calculated using:

$$C_p = \frac{P - P_A}{P_T - P_A} \qquad [1]$$

A five-hole pitot tube and a boundary layer probe with a swan neck and flattened end were used to obtain velocity profiles through several sections along the duct. The probes used standard hypodermic stainless steel tubing with an external diameter of 1.65mm and an internal diameter of 1.25mm. A Betz manometer was used to measure the pressures from the probes at various distances into the duct. Velocities were defined relative to the local top wall static pressure measurement and were obtained from the Betz manometer readings using:

$$\rho_w . g . H = \tfrac{1}{2} \rho_a . U^2$$

$$U = \sqrt{\frac{\rho_w . g . H.2}{\rho_a}} \qquad [2]$$

3.4 TESTS

Experiments were carried out at a combination of wind tunnel speeds and impeller speeds corresponding to three distinct operating regimes. These settings were based on visualisation of flow through the water-jet. The wind speed was set using the wind tunnel manometer whilst the water-jet impeller remained turned off. The impeller was then started and run up to the required speed. Upon doing this the indicated wind tunnel speed increased. Conditions of each test case are shown in Table 1. The Impeller Velocity Ratio, IVR, is defined as the ratio of mean flow speed at the duct exit to the indicated wind tunnel speed (ship speed).

Table 1 - Test Case Conditions

Test Case Number	1	2	3
Indicated Wind Speed (Impeller off)	15m/s	10m/s	10m/s
Impeller R.P.M.	950	875	1051
Indicated Wind Speed (Impeller on)	21.1m/s	14.8m/s	15.2m/s
Impeller Velocity Ratio, IVR	0.883	1.173	1.406

Under the conditions for Case 1 the wool tufts showed separation occurring on the upper duct wall and attached flow on the lower wall. For Case 2 it was seen that separation was beginning to form on the lower wall, and Case 3 indicated a definite separation on the lower duct wall. The flow along the upper wall was fairly well attached for both Cases 2 and 3.

The Reynolds number of the flow through the duct based on the exit diameter and exit speed was in the range of 0.32×10^6 to 0.37×10^6 which is at least 3 to 4 orders of magnitude lower than full scale but double that achieved in the towing tank by Okamoto[1].

3.5 PRESENTATION OF DATA

Pressure coefficient distributions along the top and lower centre-lines are shown in Figs. 4 and 5. It should be noted that the Cp values indicate the pressure relative to that at the impeller (exit) plane for each individual test case. In addition, velocity profiles were obtained through several sections along the duct using the pitot tubes in the traverse mechanism. In each case the velocity is defined relative to the local top wall static

pressure measurement. The results are given in Figs. 6, 7 and 8 as graphs of velocity ratio against distance into the duct from the upper surface. The relative measurement positions are indicated in Fig.9.

3.6 DISCUSSION OF RESULTS

Pressure Distributions:

The top centre-line Cp variations, shown in Fig.4, give a definite increase in Cp towards the inlet for increasing IVR. This indicates that, as expected, the greater the velocity ratio the greater the acceleration of the flow through the duct. For Case 1 the flow is decelerated from the free-stream value. Once the velocity ratio has been increased, in Case 2, the Cp values are greater than zero apart from acceleration around the ramp at the inlet. The highest velocity ratio, Case 3, shows another increase in the Cp values. In this case all positions exhibit a slower flow than at the exit. Also shown are the results from Okamoto[1] for an IVR of 1.056. These agree reasonably well with the wind tunnel results.

One noticeable feature on the bottom centre-line Cp variations, Fig.5, is that the Cp values are generally lower for test case 1, suggesting higher relative velocities. This agrees strongly with the fact that the flow was attached along the bottom wall during this case. The relative velocities fall slightly for Cases 2 and 3 for which some separation was occurring on the bottom wall. Another point to highlight in Fig.5 is that for each test case the relative velocities increase towards the lip of the duct. In this region the Cp values are close to zero. It was not possible to obtain a measurement at the lip due to the physical construction of the duct model.

Velocity Profiles:

The velocity profile results from test Case 1 are shown in Fig.6. Clearly indicated on the graph is the separation region towards the top wall of the duct. This area can be seen to increase from about 50mm to 130mm deep at sections A and EA. Section EA possesses a slight separation towards the lower wall of the duct. This decrease in effective flow area caused by the additional area of separation may explain the velocity increase from section A.

Fig.7 illustrates the velocity profiles for Case 2. It is clear that a zone of separation exists at the lower duct wall, and this separation appears to grow towards the impeller plane EA. The relative velocities are higher than Case 1 and, with the exception of section D, the profiles show the expected trend of increasing velocities along the duct from C to EA. The velocity profiles for Case 3 are shown in Fig.8. As for test Case 2, the separation region occurs towards the lower duct wall, although for this case it is much more pronounced. The velocity ratio in Case 3 is 1.4 and the indicated velocities are the highest of all three cases. Again, the trend is of increasing velocities along the duct, although section D shows relatively higher velocities than expected. This is thought to be due to a reduction in the effective cross-sectional area.

3.7 SUMMARY

The wind tunnel experiments proved to be an effective technique for the study of flow through this water-jet duct. Pressure and velocity distributions along and through the duct were obtained together with a visualisation of the flow's characteristics. The

resulting trends were expected and the measured velocity profiles generally agreed with what had been shown by the wool tufts.

A detailed indication as to the behaviour of the flow was therefore provided. However, much time and planning was required in order to achieve results such as these. Ideally, there are many more measurements and combinations of tests which should have been carried out, but this was not practical given the time available. Once initial geometry definitions and command files have been created, computational fluid dynamics offer the ability to obtain comprehensive solutions of the flow relatively quickly.

4. COMPUTATIONAL ANALYSIS

4.1 AIMS

The aims were to produce, using a commercially available CFD flow solver, a three-dimensional computational model of the representative water-jet duct to be validated using the data gathered from the wind tunnel tests; to investigate the influence of pitch and yaw on the inlet flow; and to expand the problem to include a surrounding hull structure in order to study interaction effects between the hull and duct.

4.2 THE CFD PACKAGE

The commercial CFD package used to model this water-jet geometry was CFX4.1-F3D[10], formerly CFDS-Flow3D. CFX is a suite of programs intended for the prediction of laminar and turbulent flow and heat transfer processes. It is a Reynolds averaged Navier Stokes flow solver which uses multi-block structured grids of hexahedral cells for modelling three-dimensional geometries. CFX consists of a number of modules for the definition of the problem, the solution, and the output of results. The modules used were:

a) **CFX-Meshbuild** - an interactive pre-processor which creates structured multi-block meshes of hexahedral cells for use by a flow solver. Blocks are defined by their vertices and edges and, providing the adjacent blocks share the same face definition, they are joined automatically,.
b) **CFX-Setup** - a command file generator. Command programs can either be written from scratch or existing programs can be modified to suit the problem being considered. The command language is a set of commands, sub-commands and associated keywords defining the nature of the flow.
c) **Frontend Module of CFX4.1-F3D** - this takes the input specification of the problem, converts it from a form convenient for the user into a form designed for efficient execution, and performs a detailed error checking before passing the data to the solver.
d) **Solution Module of CFX4.1-F3D** - a multi-block flow solver. Once the geometry file and command program have been produced they are run through this flow solver. Appendix A describes the governing equations. The generated flow characteristics are written to an output file and a dump file which can be used for post-processing.
e) **CFX-View** - a post-processor. Using data from the dump file CFX-View produces graphics outputs for screen display. In addition, files can be produced which can be used with AVS.

4.3 DEFINITION OF THE DUCT GEOMETRY

The water-jet duct shape was defined using Wolfson Unit Shipshape. Shipshape is a series of programs designed to assist the naval architect in defining, fairing and drawing a set of ship lines[12]. Three-dimensional curves are drawn by constructing cubic splines through specified sets of points and defined as either sections or longitudinals. Shipshape was used as all information that maybe needed such as offsets, point co-ordinates and slopes can be transferred into a data file and used elsewhere.

A data file from Shipshape was created which contained point co-ordinates defining vertical sections along the duct. These points were input into the interactive multi-block

grid generator, CFX-Meshbuild. The points were used to create duct sections which were joined to make blocks. These blocks were subsequently sub-divided into hexahedral cells to generate a mesh of the geometry under investigation. Initially, in order to accurately recreate the experimental set-up a wind tunnel working section was also modelled. This was to be used for validation purposes, comparing the results with experimental data gathered. For this reason air was used as the standard fluid in the CFD model.

4.4 WORKING SECTION - WATER-JET MODEL

Difficulties with the generation of the mesh occurred around the regions where the water-jet duct joined the working section, especially at the sharp lip on the bottom centre-line of the duct. In this area, and at the upstream end of the inlet where the top centre-line rises away from the working section, the grid is an awkward shape. For this reason several individual blocks had to be created and even then the subsequent cells were non-orthogonal in places. The water-jet duct was constructed of 24 blocks whilst the working section was made up of a further 60. Each block was sub-divided into smaller cells and, where required, the cells were concentrated towards areas of greater interest. The numerical model was run using the 84 block structure consisting of up to 79600 hexahedral cells. The block structure is illustrated in Fig.10 and the shape can be compared to the experimental set-up shown in Fig.3.

4.5 CFX FLOW SOLVER

A command program was created for this geometry using CFX4-Setup. The command file variables were chosen to recreate as closely as possible the experimental conditions. Incompressible, steady, turbulent flow with the default $k-\varepsilon$ turbulence model was used. The speed of flow into the working section was set to that used in the wind tunnel tests. The mass flow through the duct exit was based on the product of speed at the midpoint and the cross-sectional area. The flow through the exit plane of the working section was obtained by the use of mass continuity. A water-jet impeller operating at constant revs does not necessarily experience a constant mass flow rate through the duct, hence the thrust and inlet velocity ratio vary. However, for simplicity a constant mass flow rate through the duct exit was defined for all the CFD models. Table 2 lists the conditions defined for each case.

Table 2 - Conditions Set For Each CFD Test Case

Test Case Number	1	2	3
Working Section Inflow Speed	21.06m/s	15m/s	15.2m/s
Duct Exit Speed	18.6m/s	17.4m/s	21.3m/s
Duct Exit Mass Flow	1.123kg/s	1.051kg/s	1.286kg/s
Impeller Velocity Ratio	0.88	1.17	1.42

Some modifications to the solution strategy had to be made before a reasonable level of convergence was obtained for the solution. A more accurate, higher order than the default, discretization method was used for the k and epsilon equations. These two variables were also iterated three times within each global iteration and under-relaxation was employed for the turbulent and velocity variables. One of the most common causes of lack of convergence within CFX is due to the cross-derivative diffusion terms in the k and ε equations on non-orthogonal grids. There was a facility for under-relaxing these terms during the course of a calculation and, as the grid was non-orthogonal in

some areas, this was done for the first 150 iterations. These strategies are described in more detail in Appendix B.

The solution was seen to converge to an acceptable level (residuals of $1x10^{-3}$) after 700 iteration cycles. The code was run on a multi-user Sun Sparc 1000 with eight 60mhz processors. Output data such as pressures, velocities and local forces throughout the geometry were readily obtainable from the solution.

4.6 COMPARISON WITH EXPERIMENT

The results of the CFD model were validated by comparing them to the results obtained from the wind tunnel tests on a model of the same water-jet duct geometry. This initial CFD model having a total cell number of 79600, 10050 being within the duct, was run for the same three conditions as tested in the laboratory. Pressures were obtained along similar centre-lines and non-dimensionalised in the same manner as those in the tests (see equation 1).

Fig.11 presents both the experimental and CFD pressure distributions along the top centre-line of the water-jet duct for three inlet velocity ratios, IVR, where IVR is the ratio of the duct exit velocity to the wind tunnel flow speed (ship speed). It can be seen that the comparison with the experimental results is good. However, it is evident in all three cases that the CFD result is offset slightly from the experimental points. This was thought to be due mainly to the method used to calculate the experimental mass flow rate. This was based on the velocity at the mid point calculated relative to the top centre-line pressure P_A. The experimental tests and CFD results indicated a static pressure gradient across the exit plane at Section A. Based on a linear variation this would imply the mass flow rate used for the CFD calculation resulted in an Inlet Velocity Ratio (IVR) which was between 3% and 5% too high.

The comparison of pressure coefficients along the bottom centre-line is shown in Fig.12. The general trends agree very well and the offset is less pronounced than along the top centre-line. However, an unexpected result is the decrease in Cp towards the lip. In this area a pressure increase is more likely to be experienced as a stagnation point tends to be located in the vicinity of the lip.

4.7 EFFECT OF PITCH AND YAW

The CFD model was expanded to investigate various inlet conditions including pitch and yaw. A further two meshes were created in which the working section was lengthened, widened and three of its walls were defined as pressure boundaries, thus providing a flat plate structure around the water-jet inlet. In addition, the water-jet block structure was redefined in order to produce a more orthogonal cell structure. One model was of half the water-jet and flat plate with a symmetry plane defined along the centre-line. This model consisted of 23 blocks with up to 55720 cells, 13120 within the duct, corresponding to a full water-jet duct model of 111440 cells, and was used to solve the flow for various angles of pitch. Another geometry modelled the full water-jet duct and consisted of 27 blocks with up to 56000 cells, 18080 being within the duct. This was used to study the flow for various angles of yaw. In each model the water-jet duct consisted of 15 blocks and the remainder made up the flow domain beneath the flat plate. Each block was sub-divided into smaller cells and where required, the cells were

concentrated towards areas of greater interest. These geometries were run at the mid inlet velocity ratio of 1.17.

The influence of the number of cells on the results was investigated for the new mesh. Half duct cell numbers were varied from 6200 to 13120, corresponding to a total cell number variation of 20200 to 55720. It was found that generally the resultant pressure coefficients remained at very similar values, the maximum change being only ±0.02. The predicted forces acting on the duct, however, altered by up to 30% in some areas due to differing cell numbers. It was thought that large distortion of cells in these regions affecting the iteration of the pressure was responsible for these differences. A significant difference between the predictions by this new mesh and the initial grid was a rise in pressure towards the lip along the bottom centre-line, which was more realistic. The reason why the initial geometry predicted a decrease in Cp was put down to poor grid quality.

In addition, a significant result of increasing the number of cells was to increase the computational time and hence the real time taken for the solver to finish. This was the deciding factor as to how many iterations and cells to use for the subsequent investigations into pitch and yaw. These were chosen as 9040 duct cells and a subsequent total cell number of 27240 for the half duct model, and double these values for the full jet model. The maximum number of iterations was set as 800.

The results obtained were plotted as pressure coefficients along the top and bottom centre-lines of the duct (Figs.13, 14, 15, 16). It is important to note that pressure is defined relative to the top centre-line point at the exit plane for each case. In addition, Figs.17 to 22 present the effects of pitch and yaw on the axial, radial and angular velocities of the flow across the impeller face plane at 0.7 radius. Three angles of pitch were investigated, -7°, $+7^{\circ}$ and $+15^{\circ}$, and 5° and 10° angles of yaw were studied.

Pitch:
Figs.13 and 14 illustrate the pressure coefficient distributions. Along the top centre-line it is seen that an increase in pitch produces a decrease in the relative pressures towards the inlet. This is expected with positive pitch because the inflow is at an angle closer to that of the ramp of the duct.

The rise in Cp values towards the lip, along the bottom centre-line, for zero pitch can be seen on Fig.14. It is also predicted that the relative pressures increase towards the inlet lip due to increasing pitch. The pressures also appear to stabilise towards the duct exit with the exception of negative pitch which produces a slightly lower relative pressure at the exit.

Yaw:
Figs.15 and 16 show results for the influence of yaw. It is seen that yaw affects the pressure distribution along the whole length of the duct. The top centre-line distribution undergoes a pressure drop along its length with the exception of a slight rise past the exit. The bottom centre-line also sees a relative pressure drop along its length except for a point at x = -0.1. The influence of yaw along the entire top and bottom centre-lines is to be expected as the fluid enters the duct at an oblique angle and will be concentrated towards one side of the duct. However, the graphs show that the predicted pressure

coefficients along the top and bottom centre-lines are nearly identical for both 5° and 10° yaw. These results were double checked using a mesh with 63520 cells rather than the original 54480 cells, and the same results were predicted. Further investigations at more angles of yaw and some experimental data are required to have confidence in these results.

Impeller plane velocity distributions:
It is inevitable that the presence of pitch or yaw on the system will also effect the pressure, and hence velocity, distribution across the exit plane of the duct. Figs.17, 18 and 19 present the variations of axial, radial and angular velocities due to the effects of pitch at 0.7 radius. The angle from Top Dead Centre (TDC) is only taken up to 180° as the CFD geometry only modelled half the duct unit. It can be assumed that the flow was symmetrical about the centre-line. The effects of yaw are illustrated in Figs.20, 21 and 22.

Pitch:
An immediate observation is that for the three velocities negative pitch has the opposite effect to positive pitch. In general, greater axial velocities exist towards the upper half of the duct, as do positive radial velocities. The prediction that radial velocities are positive towards the top half but negative towards the lower half, coupled with the angular velocities, could indicate the presence of vortices within the duct which might have arisen due to the curved sides around the inlet lip. Positive pitch increases axial velocity towards the upper half, but negative pitch decreases it. However, the angular velocities are increased around the entire radius due to negative pitch.

Yaw:
Yaw produces quite different results. A major effect is the lack of symmetry around the radius. Both radial and angular velocities exhibit greater speeds offset to one side of the duct centre-line. This is expected with an oblique inflow. The axial velocity is decreased towards the top half of the duct and increased in the lower half. This is also the case for the radial velocities. Angular speeds, as with negative pitch, are increased around the entire radius again.

Table 3 lists the total forces, acting on the duct, calculated by the flow solver for the X, Y and Z co-ordinates. X being along the jet (aft to for'd.), Y is the vertical component and Z the lateral co-ordinate. Note the fluid modelled was air.

Table 3. *Total Duct Forces (N) Calculated By CFX4.1-F3D.*

Pitch	Yaw	X	Y	Z
-7	0	-0.894	-0.989	0.000
0	0	-0.766	0.786	0.000
15	0	-0.995	4.699	0.000
0	5	-1.519	2.871	-1.246

It is indicated that when the water-jet duct is subject to pitch or yaw the resistance of the unit increases, especially when yaw is imposed - in this case 5 degrees yaw almost doubled the resistance of the zero degrees case and, as expected, some lateral forces are produced. However, the duct tends to produce more lift (Y forces) with yaw, and certainly with positive pitch.

4.8 SUMMARY

The influence of pitch and yaw produces a change in the pressure distributions, hence velocity and force distributions along the duct and across the outflow plane. In reality this would impose a non-uniform flow at the face of the impeller reducing the performance. In addition, there would also be a change in mass flow rate through the duct affecting the overall thrust of the unit. However, some effects, such as the extra lift produced, may be of benefit to the overall system. For this to be observed, the whole sytsem, duct and surrounding hull, as a single unit needs to be considered.

5. INTERACTION EFFECTS

5.1 HULL-WATER-JET MODEL

In order to produce a more realistic model of an operational water-jet duct it was necessary to model a hull shape around the inlet rather than a flat plate. To reduce computational time only the aft half of a hull was modelled. This assumed that the upstream influence of the water-jet was negligible over the forward part of the hull. The hull was based upon a Series 64 hull[13] as similar jet-hull configurations are in operation and data on this hull was readily available.

Point co-ordinates defining sections along the hull were input into CFX-Meshbuild. Splines were created between the points to define sections, and blocks were created externally of these sections to define the flow domain beneath the hull. The structure is shown in Fig.23. At present, the hull shape has not been optimised to accept the water-jet inlet, it is defined up to the water-line and no free surface effects have been taken into account. It was assumed that the influence of the water-jet on the hull bottom would not strongly influence wavemaking resistance.

Pressures along the duct and forces on the water-jet and hull were obtained for an inlet velocity ratio of 1.17. In addition, the bare hull alone was run at the same flow conditions in order to directly compare the frictional and pressure forces acting on the hull with and without a water-jet.

Fig.24 shows the predicted top centre-line pressure coefficient distribution for the flow through the duct in the presence of the hull. It is seen in Fig.24 that the top centre-line relative pressures rise towards the inlet of the duct but soon settle to very near the original values without the hull. This rise might be due to the possible growth of a boundary layer along the hull or the slight change in angle between the hull and the ramp. This angle was greater for the flat plate case. The hull influence on the bottom centre-line pressure distribution is illustrated in Fig.25. The predicted results indicate a decrease in relative pressures, from the flat plate case, at the lip, but a general increase through the duct is evident. The resistance forces acting on the duct unit did not alter significantly due to the presence of the hull, however, the solver predicted that the duct would produce more lift.

These hull effects suggest that if a water-jet duct is to be designed for a specific application, not only does the flow through the duct have to be studied, but the additional influence of the surrounding hull must also be taken into consideration.

5.2 THRUST DEDUCTION

The flow over the hull in the vicinity of the water-jet intake is disturbed due to the suction. The boundary layer ahead of the lip is likely to be absorbed by the jet and a new boundary layer will develop on the hull behind the stagnation point on the intake lip. Vortices are also likely to occur at the corners where the duct joins the hull. Consequently there will be a difference between the bare hull resistance and the resistance of the hull with the water-jet present. This difference is commonly expressed as a Thrust Deduction Factor, t;

$$T(1-t)=R_{BH} \qquad [3]$$

where $T = \dot{m}(V_e - V_i)$ [4]

Table 4 lists the total forces in the X, Y and Z co-ordinates, including viscous and pressure form resistance, calculated by the flow solver for two IVR's. Note that the fluid used in this case was air and only the aft half of the hull is considered.

Table 4. Forces Calculated By CFX4.1-F3D.

Total Forces (N) IVR=1.17	X	Y	Z
Hull Alone (no duct)	-2.487	-2.919	0.0003
Hull Forces + Duct Inlet [a]	-2.784	-2.967	0.0004
Hull Forces + Duct Forces [b]	-3.562	-1.262	-0.0069
Total Forces (N) IVR=1.25	**X**	**Y**	**Z**
Hull Alone (no duct)	-2.487	-2.919	0.0003
Hull Forces + Duct Inlet [a]	-2.791	-2.924	0.0006
Hull Forces + Duct Forces [b]	-3.522	-1.043	-0.0028

Superscript 'a' denotes the hull with the water-jet inlet, but without the duct forces being taken into account. Superscript 'b' denotes the hull with the duct, including the forces in the duct.

From these results it is possible to see how the presence of a water-jet duct affects the overall forces in the system. The resistance of the system is increased and the force in the Y direction also increased suggesting the duct provides some lift. The equivalent total forces for a higher inlet velocity ratio are also presented. Again, the presence of the duct affects the forces in the same manner. The values do not alter significantly for the higher IVR, however, the resistance of the hull and duct is slightly lower at the higher IVR, possibly suggesting better flow through the duct, and the duct also appears to produce more lift.

Using Series 64 data[13] it was calculated that for the hull in air, its total bare hull resistance, R_{BH}, was 5.7N. The CFD analysis calculated the resistance of the aft half of the bare hull to be 2.49N. Subtracting this from the Series 64 bare hull resistance gave a value for the forward bare hull and total wavemaking resistance, R_{FW}, of 3.22N. Assuming the forward hull and wavemaking resistance remained constant for the hull with and without the water-jet, a value for the total resistance of the hull with the water-jet, R_T, could be calculated using:

$$R_T = R_{FW} + R_{CFD} \quad [5]$$

where R_{CFD} was the resistance calculated by the flow solver for the aft hull with the presence of the water-jet. Table 5 shows the results.

Table 5. Resistance Calculations.

IVR	R_{FW} (N)	R_{CFD}^a (N)	R_{CFD}^b (N)	R_T^a (N)	R_T^b (N)	t^a	t^b
1.17	3.22	2.78	3.56	6.00	6.78	0.05	0.15
1.25	3.22	2.79	3.52	6.01	6.74	0.05	0.15

Superscript 'a' denotes the hull with the water-jet inlet, but without the duct forces being taken into account. Superscript 'b' denotes the hull with the duct, including the forces in the duct.

Assuming the additional thrust produced by the water-jet pump delivered the correct amount for the self propulsion condition, i.e. the total resistance R_T equated to the thrust, T, a thrust deduction factor, t, was calculated using equation 3.

The calculated thrust deduction factors are also shown in Table 5. There are two values given for each IVR, the first neglecting the duct resistance, the second including the duct resistance. Based on the assumptions given, the results indicate that an augment of up to 15% thrust is required to propell the vessel at the original bare hull speed due to interaction effects at the given IVR's.

5.3 SUMMARY

The study of interaction effects above is only a simple calculation, based on the given assumptions, in order to obtain an idea of the effects on the required thrust. There is still some argument as to how thrust deduction should be calculated for water-jet propelled craft and little data has been published on it. Past measurements and predictions of interaction effects have, in some cases, suggested they increase hull resistance whilst, in other cases, decrease resistance. Van Terwisga[14] indicated a thrust deduction factor ranging from +20% to +0.5% for one hull form, but for another hull, a range of +5% to -4%, varying with ship speed. Coop and Bowen[15] illustrated similar findings. It appears thrust deduction factors vary with hull form, water-jet geometry and ship speed. This emphasises the importance of modelling the hull form around the duct. It is likely that other physical factors, such as the alteration of the stern wave system by the jet of water play an important part in the overall calculation of t.

6. DISCUSSION OF PRACTICAL IMPLICATIONS

The aim of the work has been to develop a three-dimensional RANS computational model of a representative water-jet inlet duct and upstream hull. The report has described the various stages taken and the results obtained whilst achieving this goal.

Once a robust and reliable solution strategy had been created, much of the work concentrated on the geometry definition of the CFD model, and attempts were made to produce a more orthogonal mesh. It has been demonstrated that the mesh, although still not optimised, can produce reasonable solutions. However, with the exception of the initial duct and working section CFD model, the results obtained from the flow solver have not been validated. This was due to lack of experimental data. They have been judged instead, on what might be expected to happen when subject to pitch, yaw and the influence of a hull. More experimental data is required.

Benefits of CFD include the ability to carry out numerous tests at the design stage without the need to reuse expensive experimental facilities, and the influence of differing flow conditions and hull/duct shapes can be studied relatively quickly. A comprehensive solution of the problem can be obtained which provides the engineer with properties of the flow such as velocity profiles, pressure distributions and subsequent forces. However, at present there are limitations to using such CFD packages. The ability to achieve a good geometry definition of a complex 3-dimensional water-jet duct, or even alter it slightly can be difficult and time consuming. In addition, the solutions require fast computers and much computer memory. Fig.26 illustrates the computing time required for 800 iterations of a water-jet geometry with differing number of cells, the solver was run on a multi-user Sun Sparc 1000 with eight 60mhz processors. There is an obvious and expected rise in computational time with number of cells, and because of this there is often a compromise between the cell numbers used for an accurate solution and the time available. The real-time necessary on the multi-user system for the flow solver was up to four times the CPU time.

Some precautions must also be taken firstly, to define the initial boundary conditions accurately and , secondly, to have some means of validation. The CFD results cannot be assumed to be correct unless some validation has been employed, usually by means of experimentation. As it becomes possible, with improvements in computational capacity, to run problems with larger numbers of cells the critical influence of the turbulence model also needs to be investigated in detail.

It has been calculated by the flow solver how differing inflow conditions into the pump affect the pressure and velocity distributions at the impeller face. How this would affect the performance of the pump, and thus the overall propulsion system, is uncertain. The characteristics of the pump therefore need to be investigated. However, for a CFD code to solve the flow for the unit as a whole (hull + duct + pump) there would be too much computational power and time required. For this reason it should be beneficial to model the pump alone with the, already predicted, inflow conditions imposed on it.

7. CONCLUSIONS

1. The use of a wind tunnel is an effective technique for investigating water-jet duct inlet flows. The experimental facility developed provides a reliable method for generating accurate data for numerical validation studies. However, much time is required to obtain a good data base of results.
2. More experimental data is required to be used as a basis for further CFD validation studies.
3. CFD codes allow a comprehensive solution of the flow to be obtained relatively quickly. There is also a quick turn-around between tests and the influence of different inlet flow conditions can be studied relatively easily.
4. The computational model of the representative water-jet duct produced good results which gave a reasonable correlation with experimental data. There was a slight offset between the results due to differences in mass flow rate.
5. Although the model calculated reasonable predictions for the influence of pitch and yaw, further validation work for these cases is necessary.
6. The generation of the water-jet duct and hull topology is a time consuming process. However, it has been shown that the hull's influence must be considered when investigating the performance of a water-jet duct.
7. A further study into the flow through the pump would lead to more understanding of how the performance of the whole unit (hull+duct+pump) is affected by different operating conditions.
8. There is often a compromise between accuracy, number of cells and time available for a CFD run.
9. The potential benefits to the engineer of using such CFD flow solvers during the initial design stages of a water-jet duct have been illustrated. In particular, the ability to obtain detailed surface pressure and viscous force distributions allows a far greater understanding of the resistance and propulsion aspects of using water-jets.

REFERENCES

1. OKAMOTO Y, SUGIOKA H, KITAMURA Y - "*On the Pressure Distribution of a Water-jet Intake Duct in Self Propulsion Conditions.*" Second International Conference on Fast Sea Transportation, (Fast'93) pp843-853.

2. PYLKKANEN JV - "*Design of Water-jet Inlet: Selection of Main Dimensions and Two-Dimensional Diffuser and Lip Section Shape.*" VTT Manufacturing Technology, Technical Report VALB-29. 1994.

3. PYLKKANEN JV - "*A Test Case of the Application of a CFD Code for Predicting Water-jet Inlet Flow.*" 21st International Towing Tank Conference. Supplement to the report of the Water-jets Group. 1996.

4. DAI C, KERR C, NGUYEN P, WANG H - *"A Novel Flush Inlet Design Methodology for Water-jet Propulsion.*" Third International Conference on Fast Sea Transportation, (Fast'95) pp1367-1378.

5. MOSS.R - "*Wind Tunnel Modelling Of A Water-jet Propulsion System.*" University Of Southampton, Department Of Ship Science, M.Sc. Thesis, Jan.1995.

6. PEASE.M.R - "*The Design And Development Of A Model Water-jet Impeller.*" University Of Southampton, Department Of Ship Science, M.Sc. Thesis, Oct.1995.

7. ENGLISH EG - "*An Investigation Into the Computer Modelling of a Water-jet Propulsion Unit.*" University Of Southampton, Department of Ship Science, B.Eng. Honours Report, 1994/95.

8. HUGHES A.W. - "*Computation and Validation of the Flow Through an Inlet Duct of a Representative Water-jet.*" University of Southampton, Department of Ship Science, B.Eng. Honours Report, May 1996.

9. ALLISON J - "*Marine Waterjet Propulsion.*" Trans. SNAME, Vol.101, pp275-335. 1993.

10. "*Environment User Guide", "CFDS-Flow3d User Guide*" and "*CFX4.1 User Guide.*" UK AEA TECHNOLOGY, Harwell. 1995.

11. TAN M Y - "*Application of CFD to Marine Dynamics.*" University of Southampton, Department of Ship Science, Lecture notes, 1996.

12. "*Shipshape Manual- Version I.*" WOLFSON UNIT FOR MARINE TECHNOLOGY AND INDUSTRIAL AERODYNAMICS. 1990.

13. HUGH YH Yeh - "*Series 64 Resistance Experiments on High-Speed Displacement Forms.*" Marine Technology, July 1965.

14. van TERWISGA T - "*The Effect of Waterjet-Hull Interaction on Thrust and Propulsive Efficiency.*" First International Conference on Fast Sea Transportation, (Fast'91). pp1149-1167.

15. COOP HG, BOWEN AJ - "*Hull-Waterjet Interaction Mechanisms: Theory and Validation.*" Second International Conference on Fast Sea Transportation, (Fast'93).pp855-866.

16. TURNOCK SR, HUGHES AW, MOSS R, MOLLAND AF - "*Investigation of Hull-Water-jet Flow Interaction.*" Fourth International Conference on Fast Sea Transportation, (Fast'97). Vol 1, pp51-58. Sydney, July 1997.

17. SEIL GJ, FLETCHER CAJ, DOCTORS LJ - "*Optimisation of Water-jet Inlets Using Computational Fluid Dynamics.*" Fourth International Conference on Fast Sea Transportation, (Fast'97). Vol 1, pp59-64. Sydney, July 1997.

18. van TERWISGA T - "*A Parametric Prediction Method for Water-jet Driven Craft.*" Fourth International Conference on Fast Sea Transportation, (Fast'97). Vol 2, pp661-667. Sydney, July 1997.

19. ROBERTS JL, WALKER GJ, DAVIS MR - "*Flow Distribution at Water-jet Intakes.*" Fourth International Conference on Fast Sea Transportation, (Fast'97). Vol 2, pp669-675. Sydney, July 1997.

20. KASHIWADANI T - "*On the Design Method of Water-jet Inlet for the SES 'Meguro 2'.*" Fourth International Conference on Fast Sea Transportation, (Fast'97). Vol 2, pp677-684. Sydney, July 1997.

21. TURNOCK SR, HUGHES AW - "*Evaluation of a CFD Code for Investigating Hull - Water-jet Flow Interaction.*" International Conference on Power, Performance and Operability of Small Craft. Southampton, 15&16th Sept.1997.

22. FITZSIMMONS PA - "*The Analysis of Water-jet Units.*" The Institute of Marine Engineers, 15th Apr.1997.

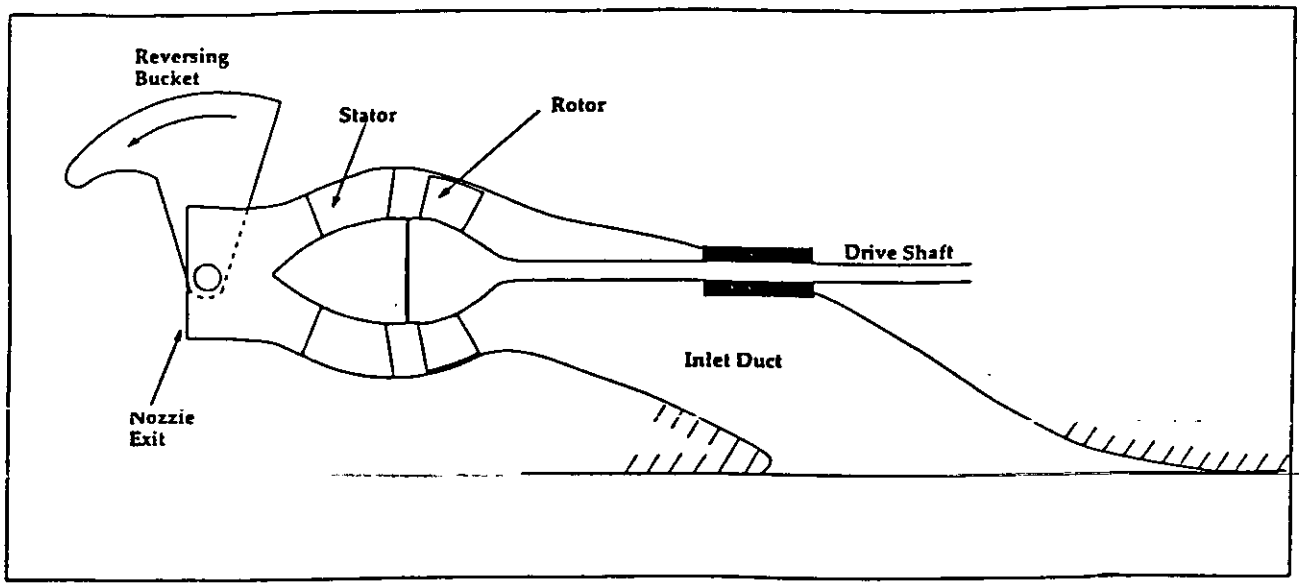

Fig.1. Schematic diagram of the components making up a typical water-jet.[22].

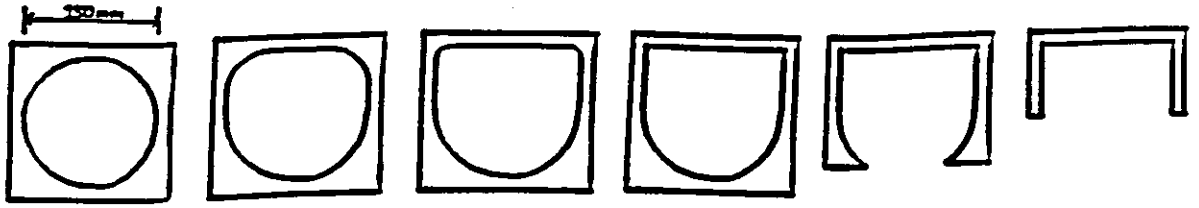

Water-jet duct section shapes.

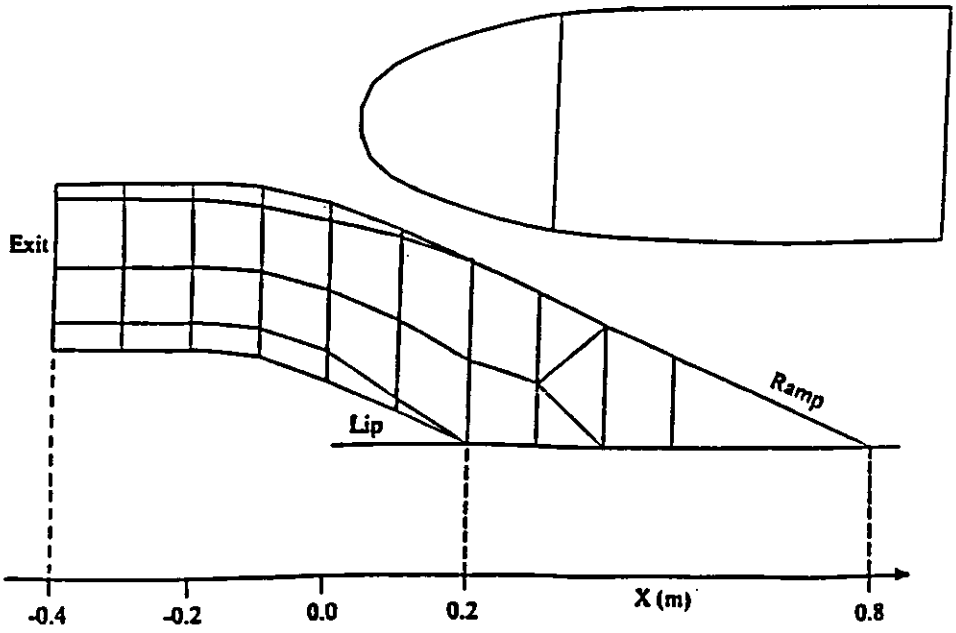

Fig.2. The representative water-jet duct geometry.

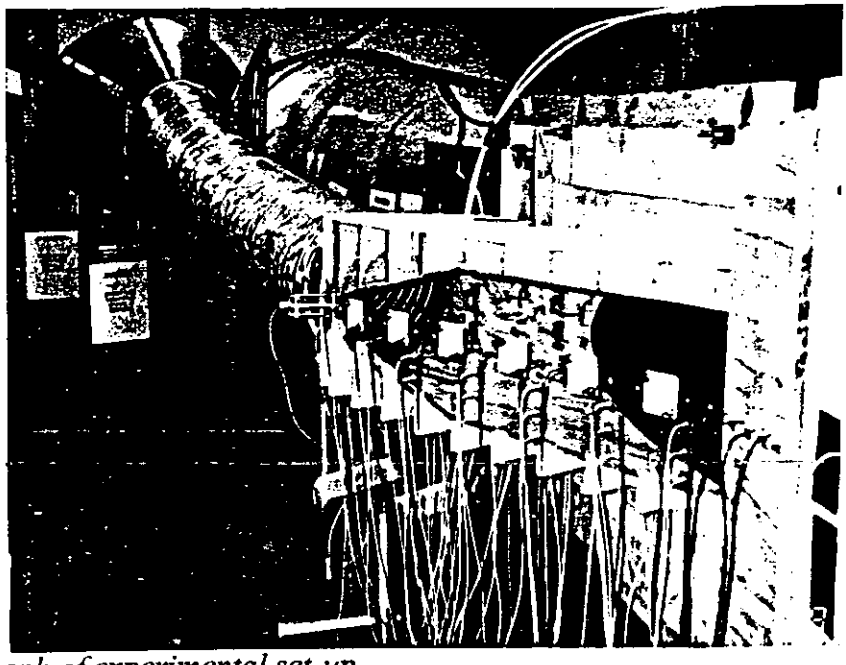

Fig.3. Photograph of experimental set-up.

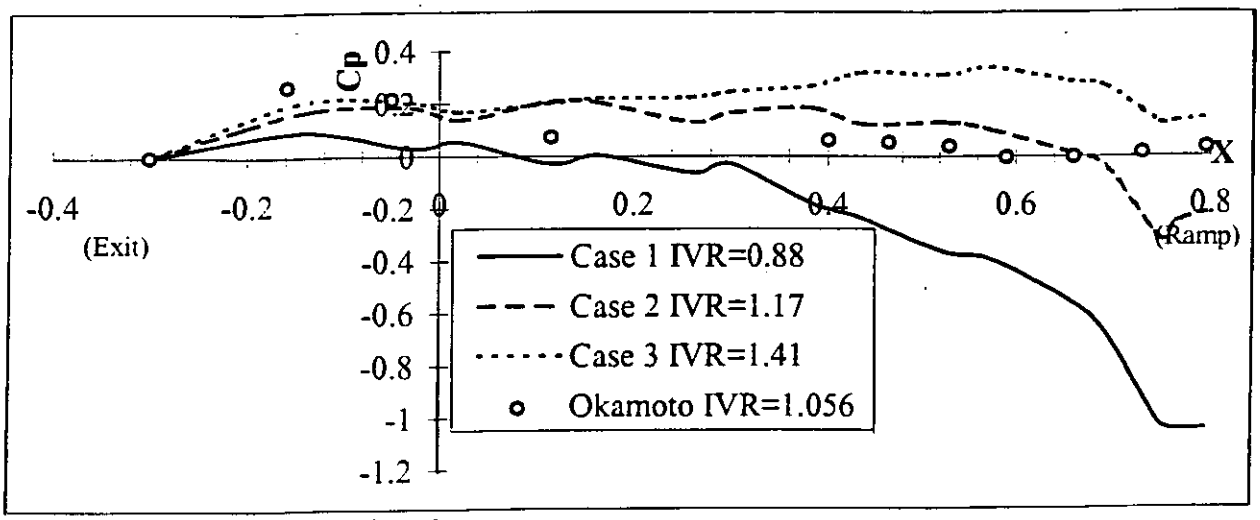

Fig.4. Top centre-line Cp distribution.

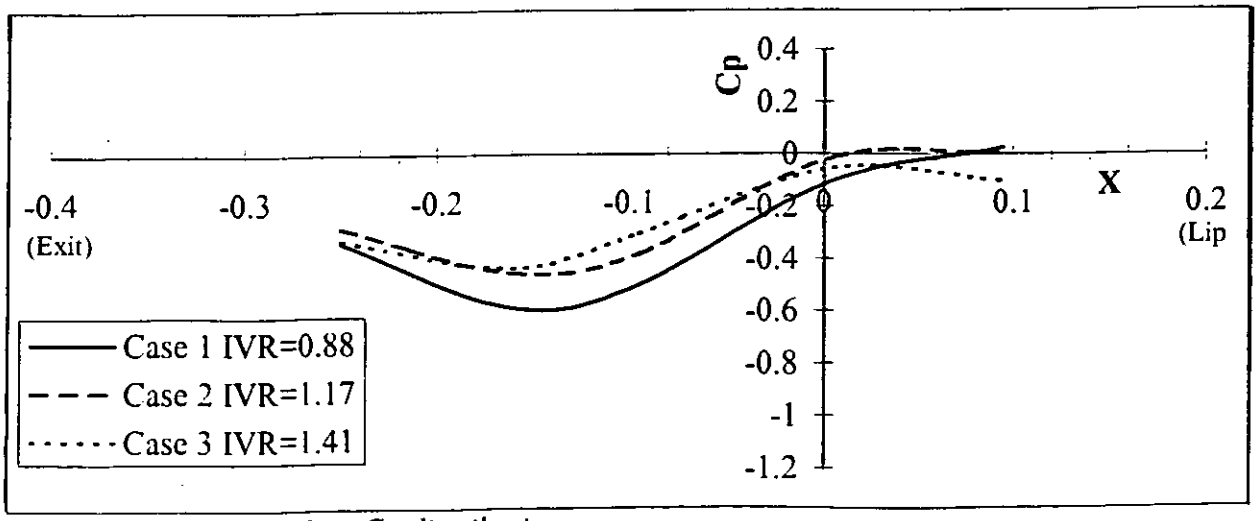

Fig.5. Bottom centre-line Cp distribution.

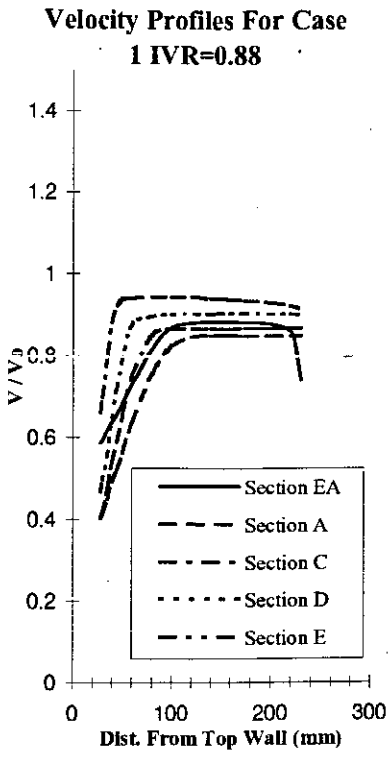

Fig.6.

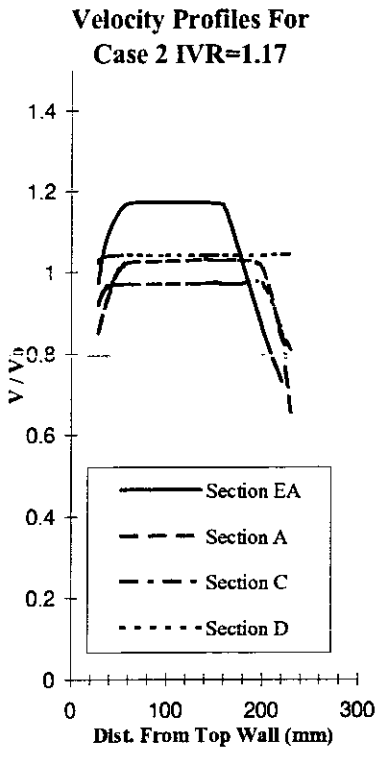

Fig.7.

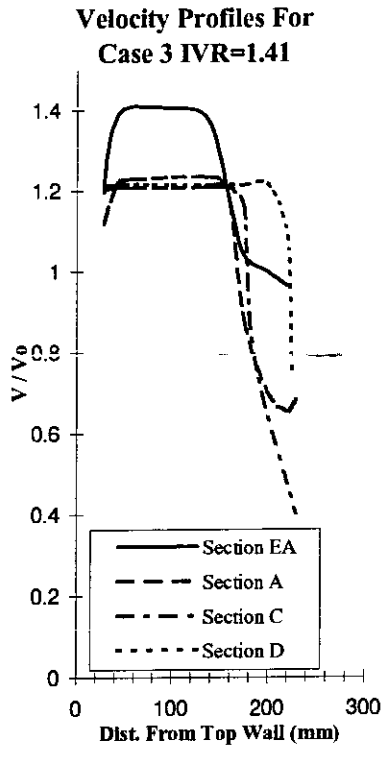

Fig.8.

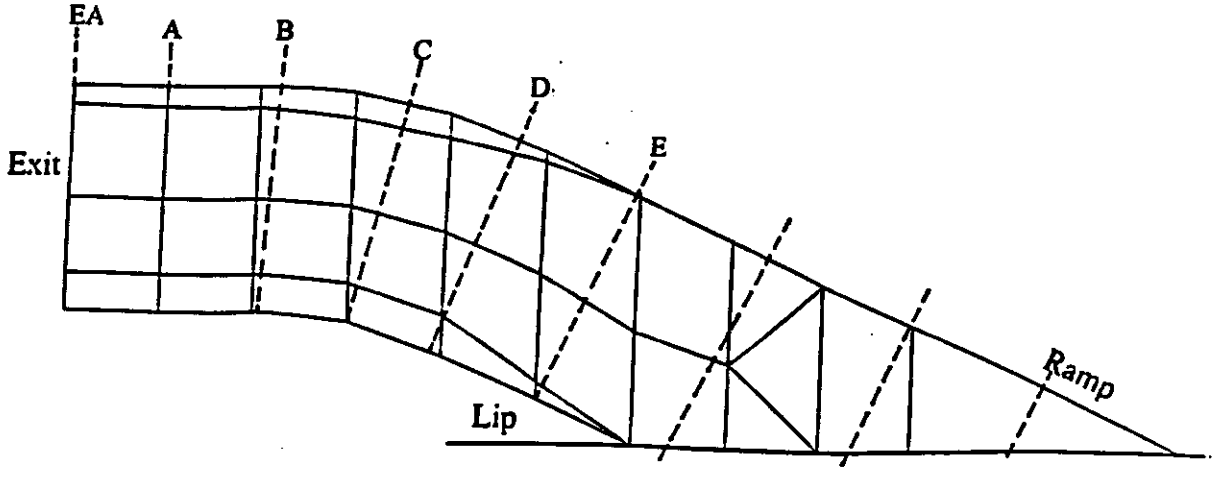

Fig.9. Relative section positions.

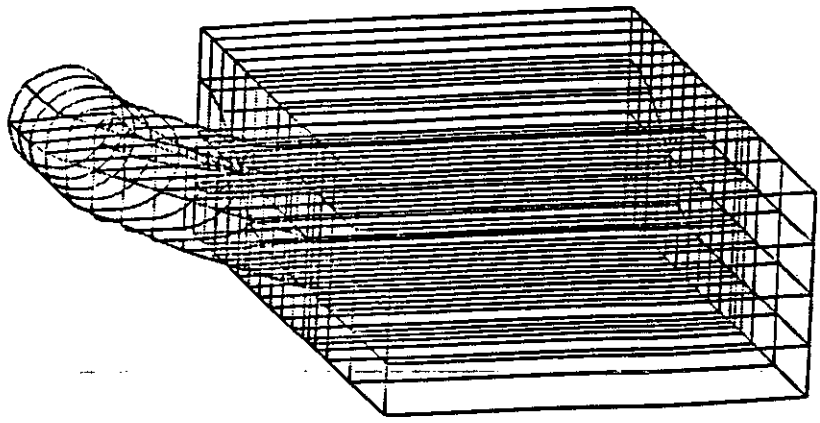

Fig.10. Block structure of water-jet duct + wind tunnel working section.

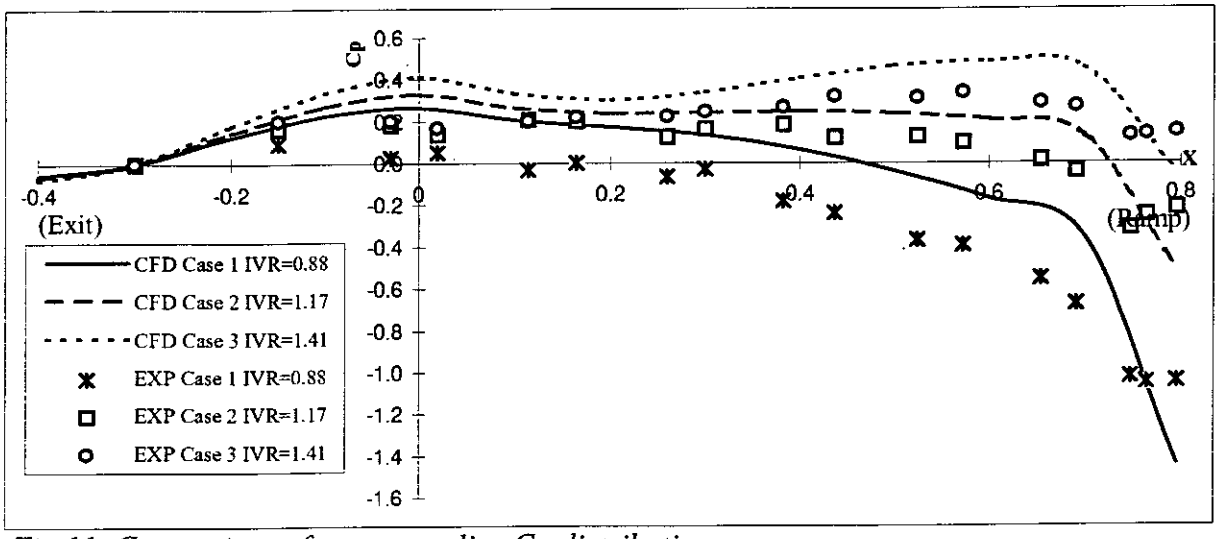

Fig.11. Comparison of top centre-line Cp distributions.

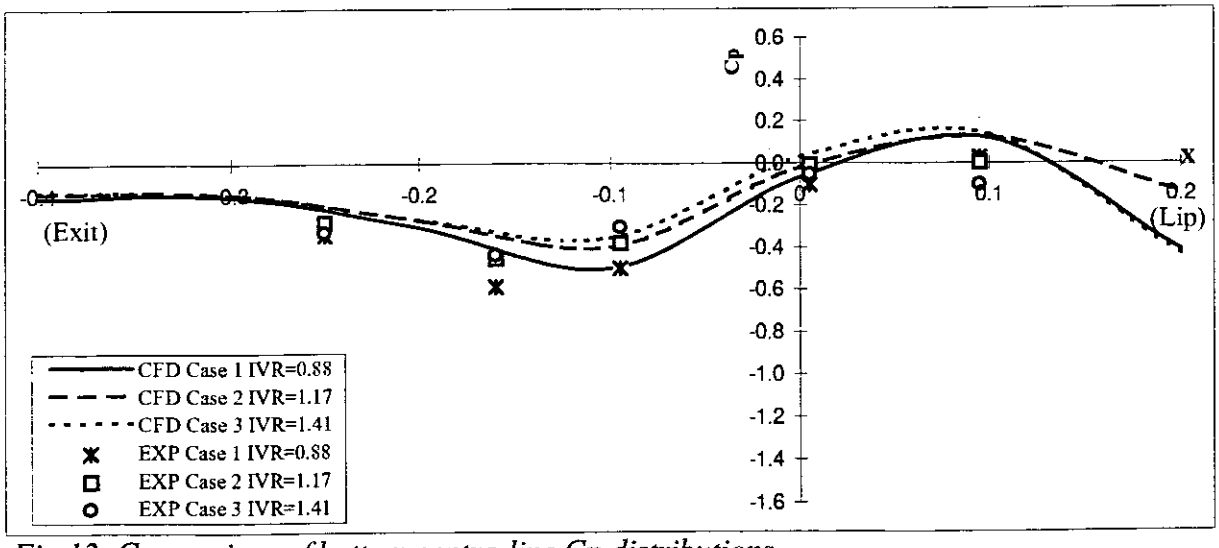

Fig.12. Comparison of bottom centre-line Cp distributions.

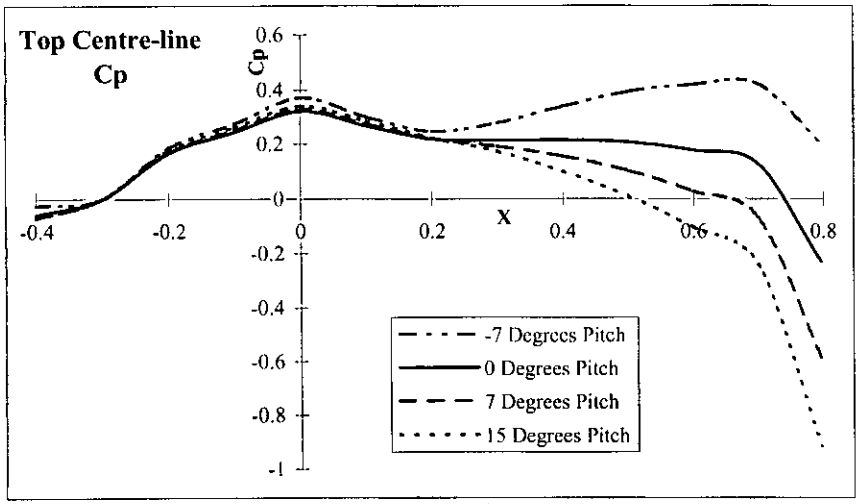

Fig.13. Influence of pitch (IVR=1.17).

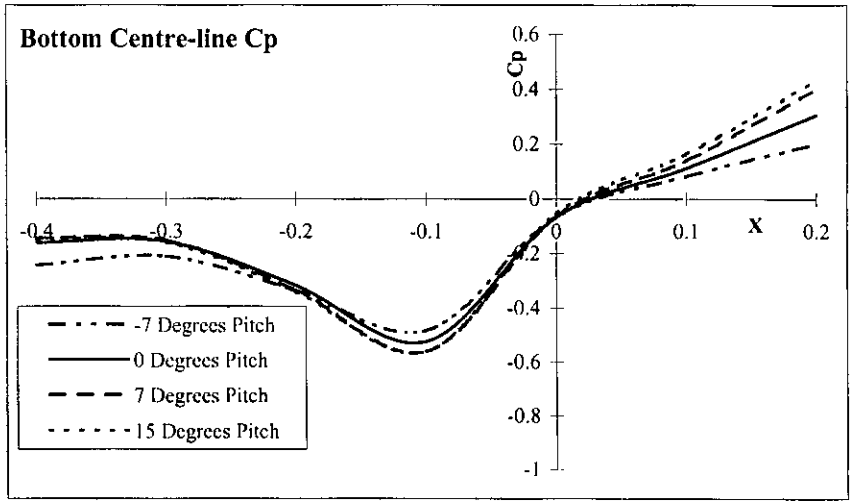

Fig.14. Influence of pitch (IVR=1.17).

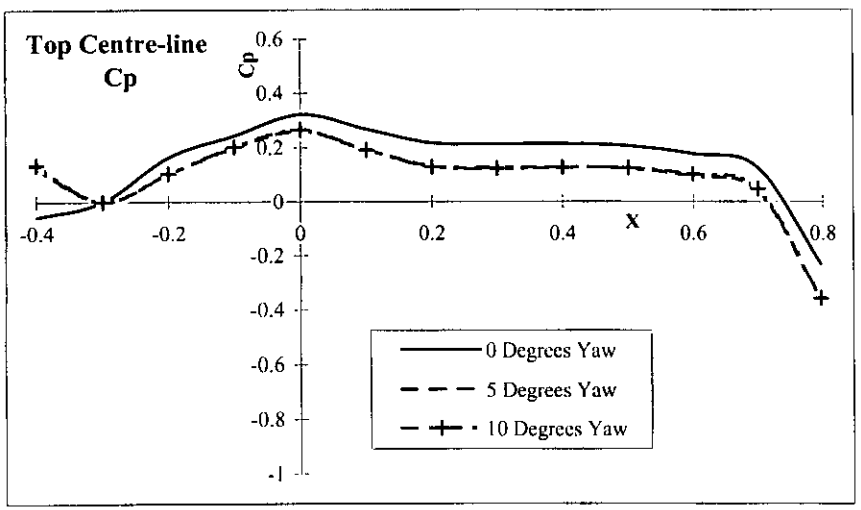

Fig.15. Influence of yaw (IVR=1.17).

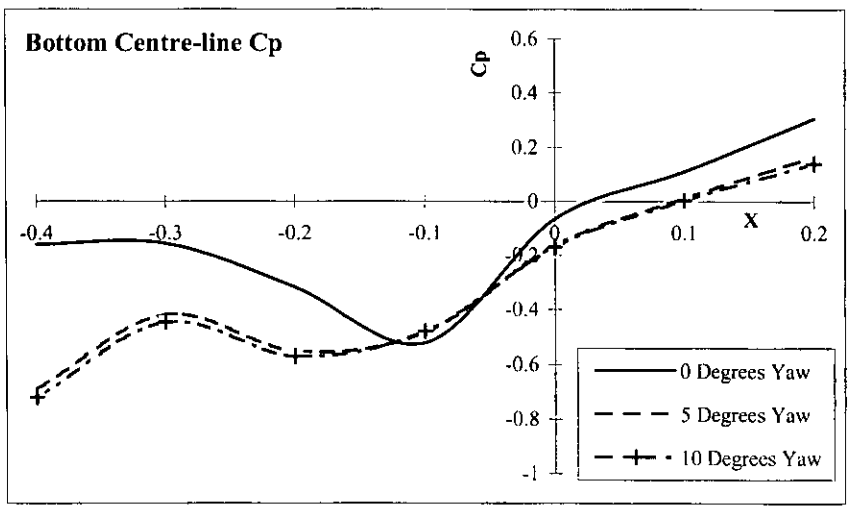

Fig.16. Influence of yaw (IVR=1.17).

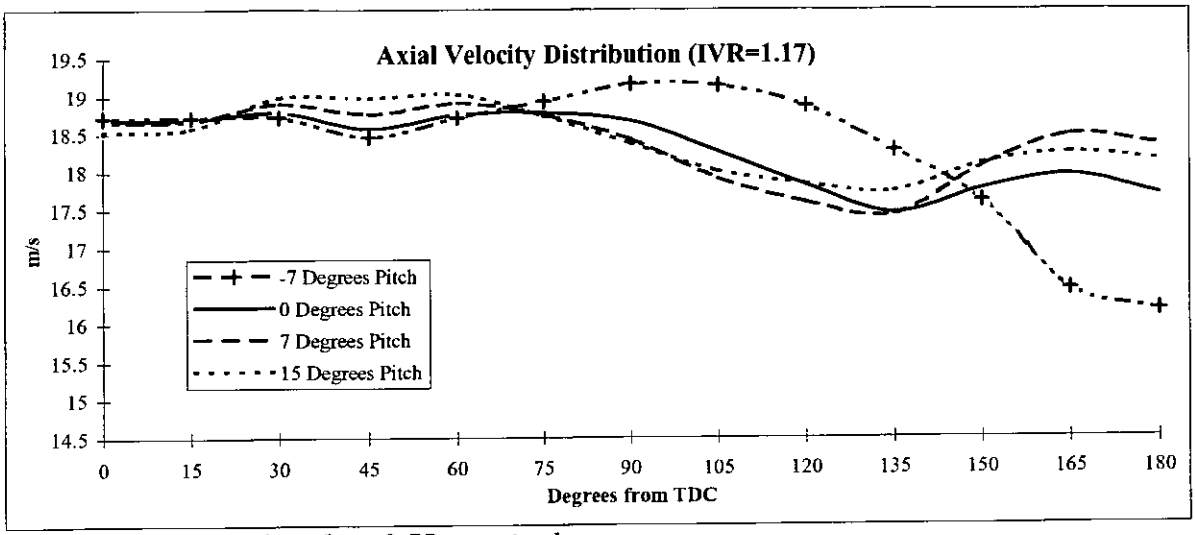

Fig.17. Influence of pitch at 0.7R at exit plane.

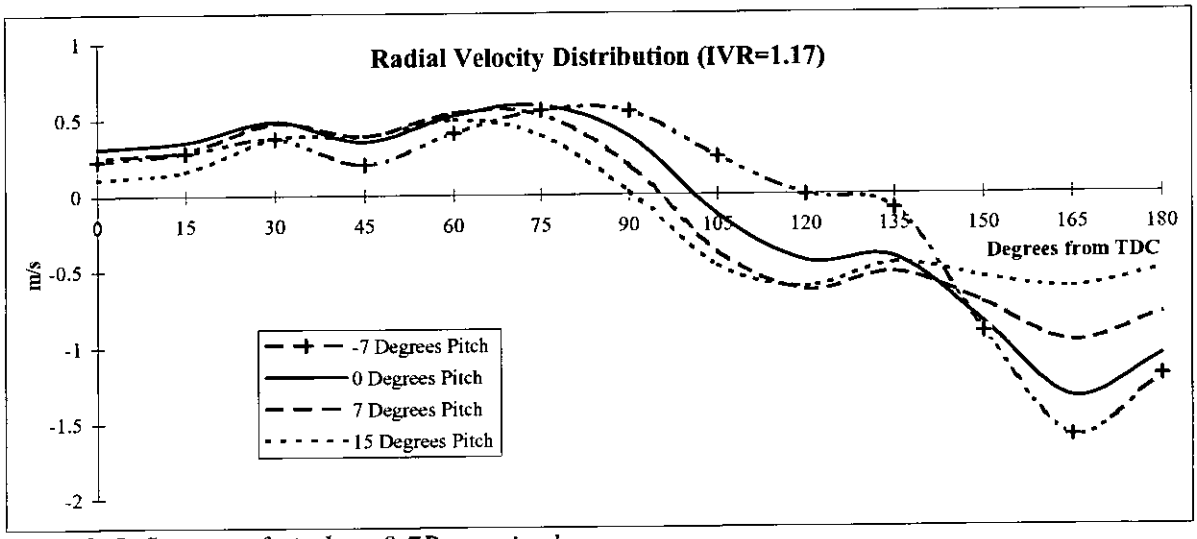

Fig.18. Influence of pitch at 0.7R at exit plane.

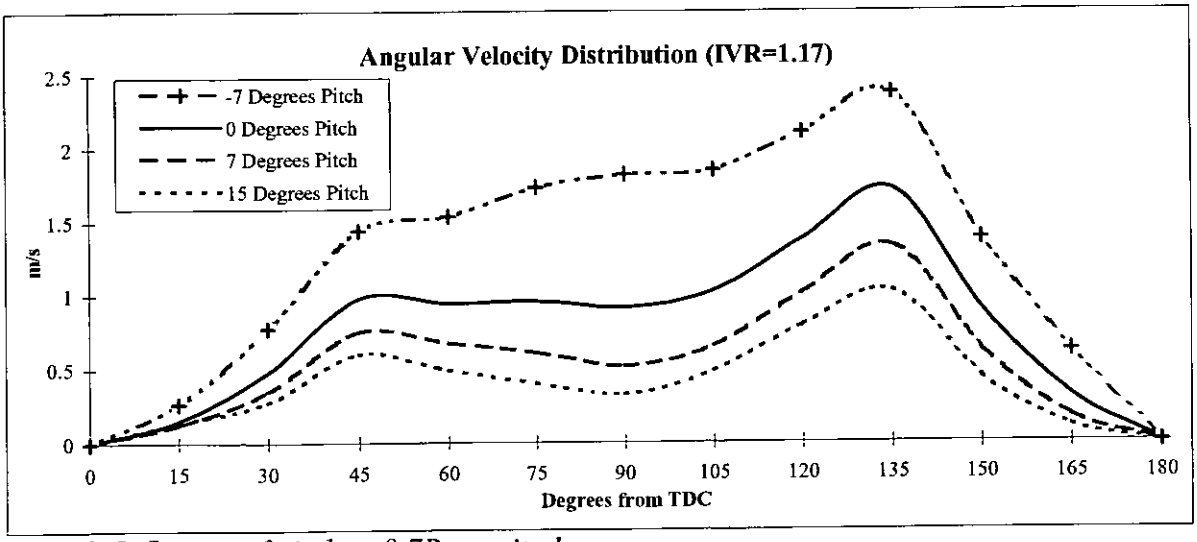

Fig.19. Influence of pitch at 0.7R at exit plane.

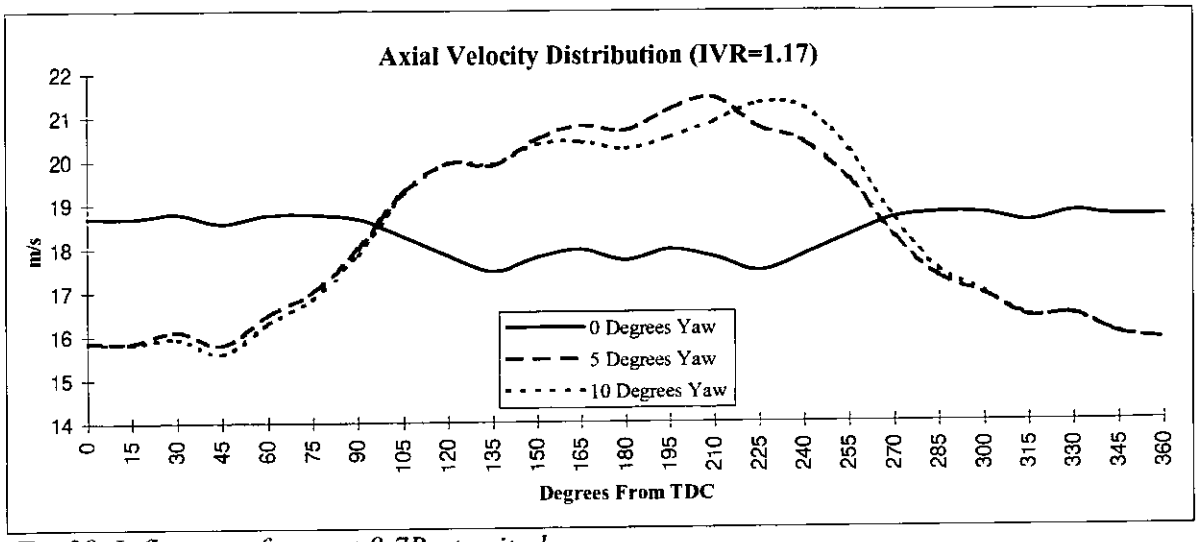

Fig.20. Influence of yaw at 0.7R at exit plane.

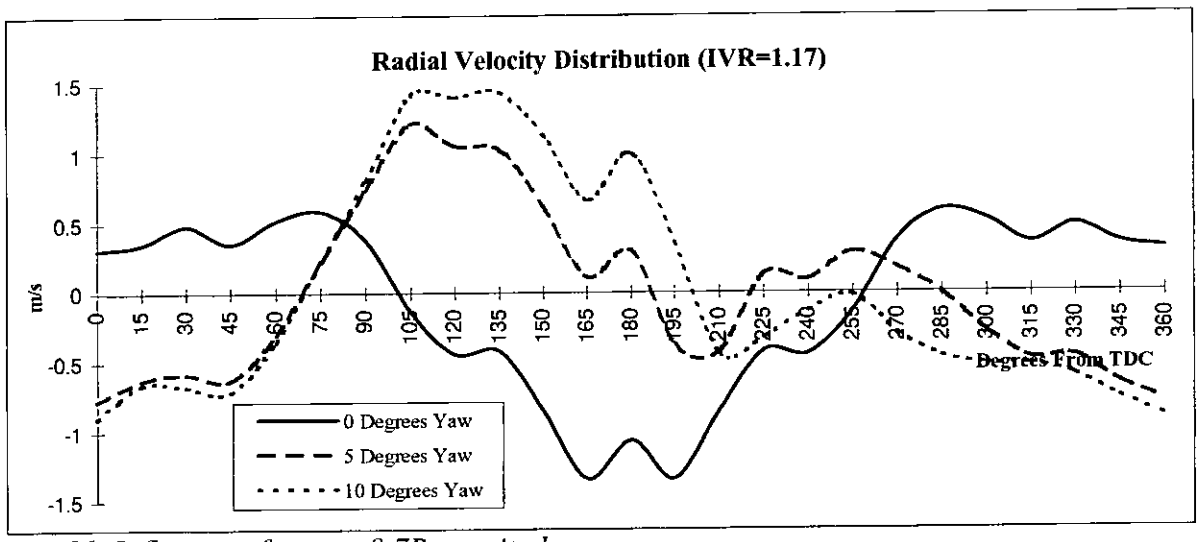

Fig.21. Influence of yaw at 0.7R at exit plane.

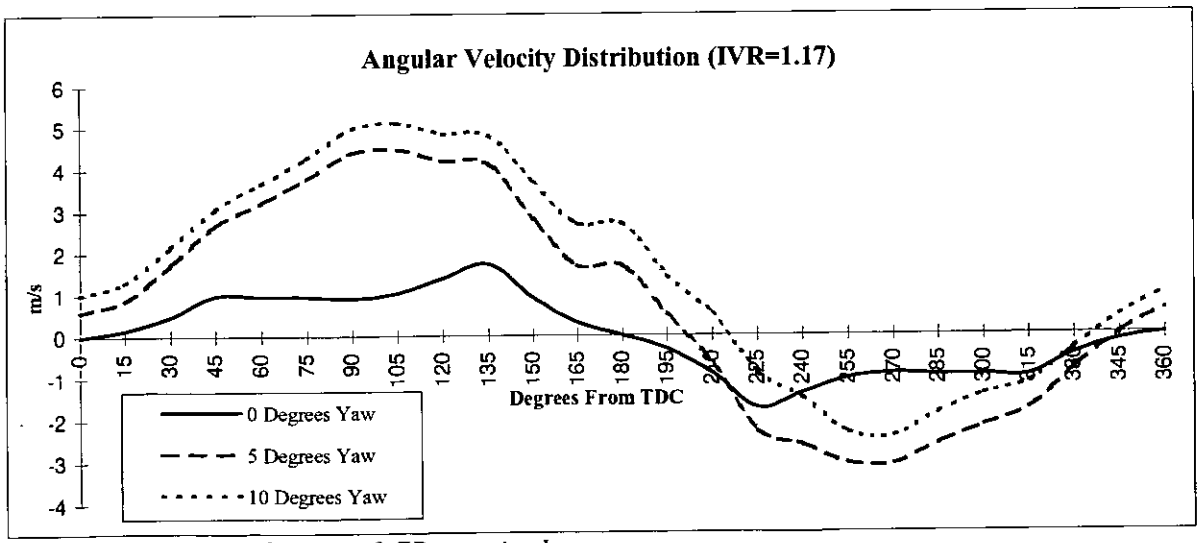

Fig.22. Influence of yaw at 0.7R at exit plane.

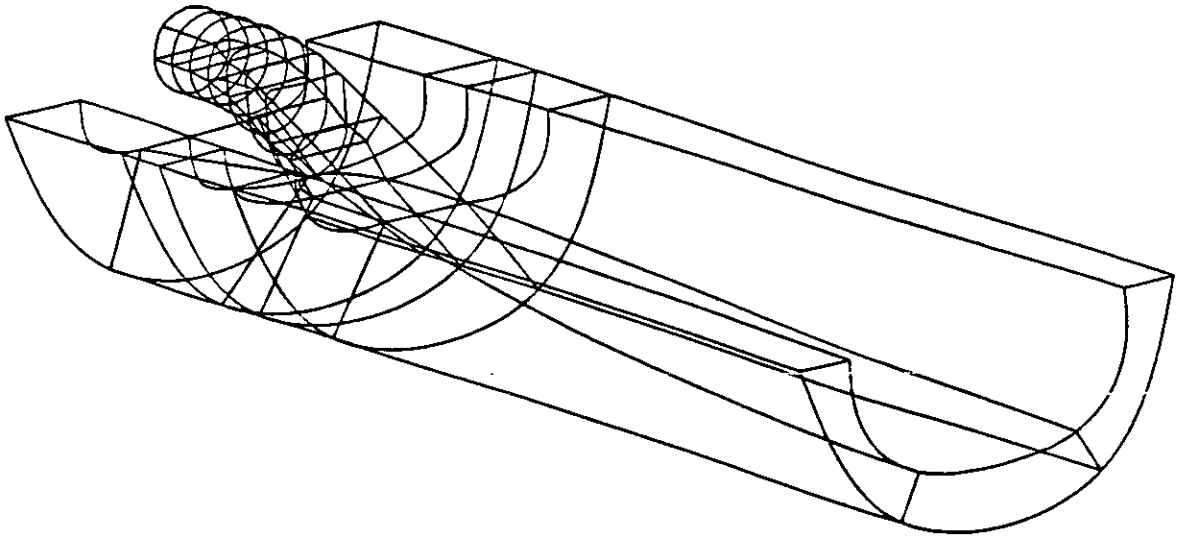

Fig.23. Structure of water-jet duct + aft half of hull.

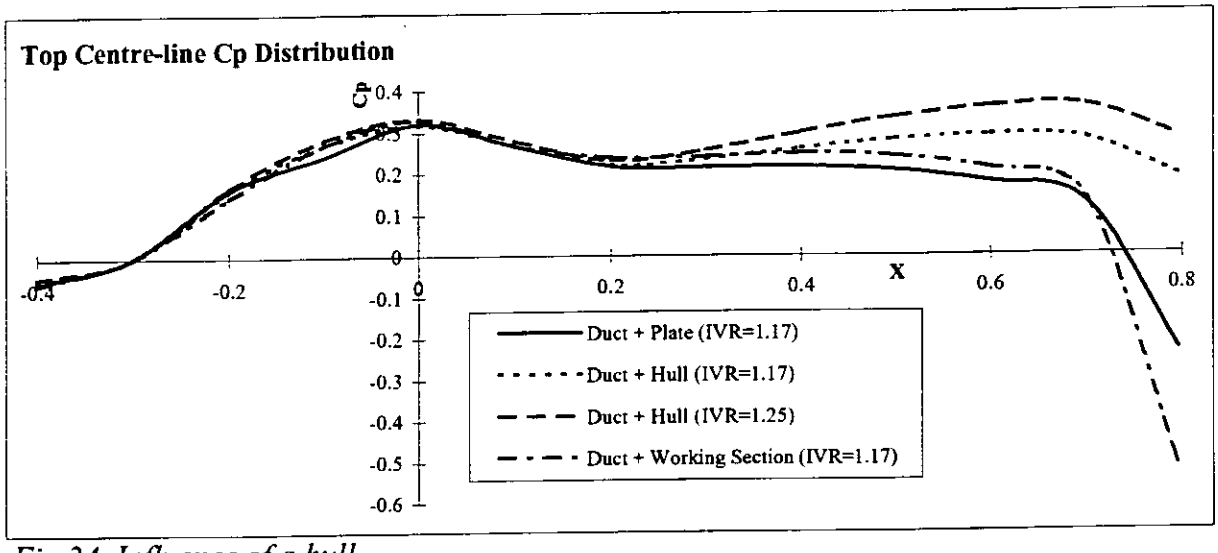

Fig.24. Influence of a hull.

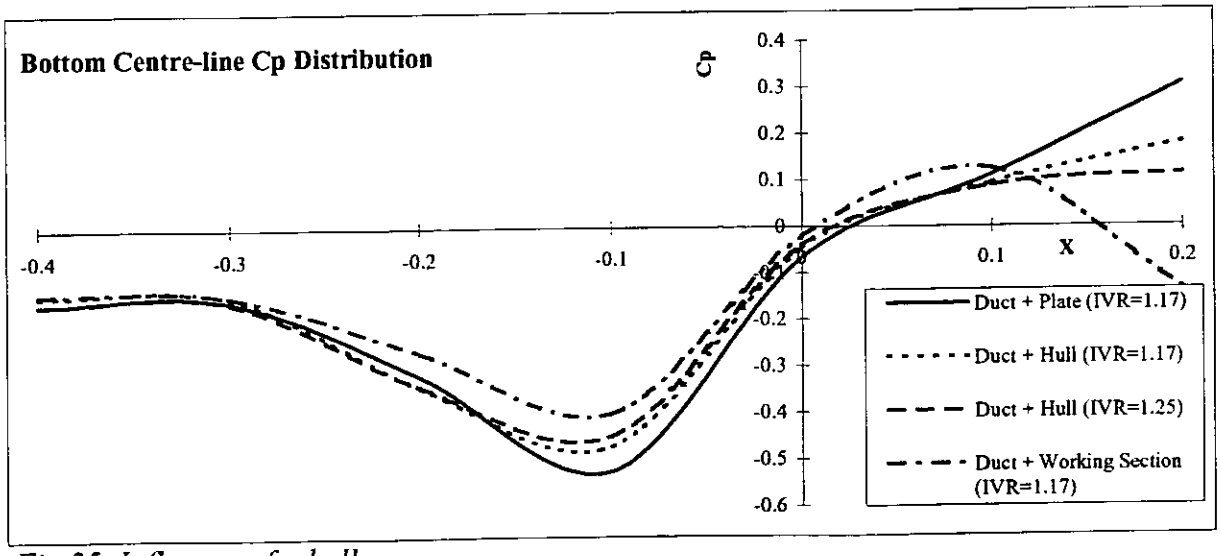

Fig.25. Influence of a hull.

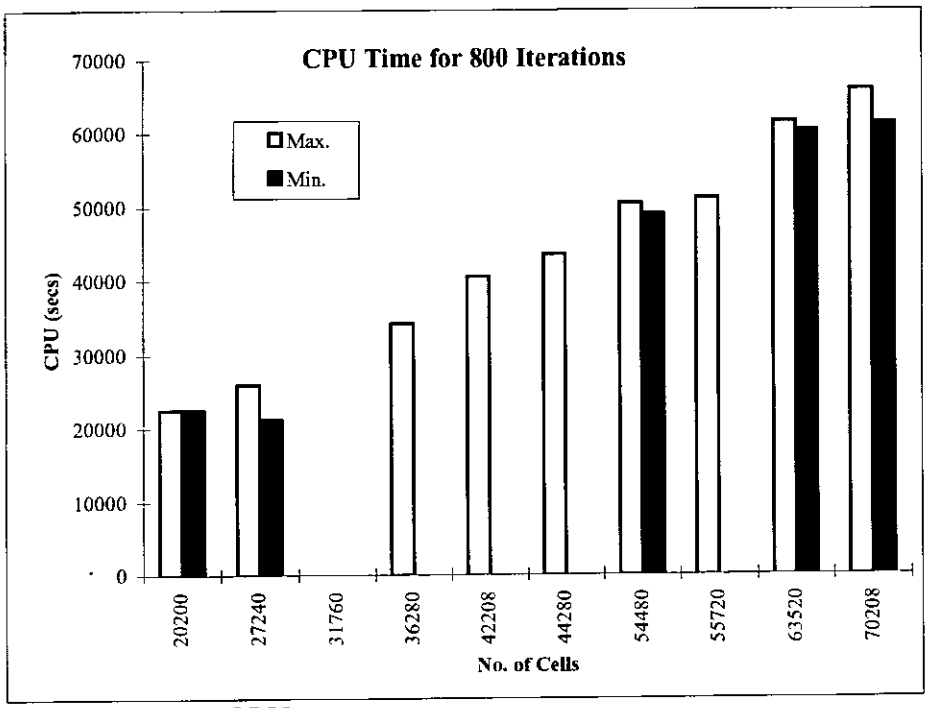

Fig.26. Number of cells vs CPU time.

Appendix A

CFX4.1-F3D Governing Equations

NOMENCLATURE

B	Body force.
H	Total enthalpy.
h	Static enthalpy.
p	Pressure.
R_n	Reynolds number.
S	Source or sink term representing creation or destruction of Φ.
T	Temperature.
t	Time.
U	Overall fluid velocity.
u	Fluid velocity in the x direction.
v	Fluid velocity in the y direction.
w	Fluid velocity in the z direction.
Γ	Diffusion coefficient.
λ	Thermal conductivity.
μ	Absolute viscosity.
υ	Kinematic viscosity.
ρ	Density.
σ	Stress.
Φ	A function of either mass, momentum or heat.

GOVERNING EQUATIONS [10,11]

There is a basic set of equations which the program solves for laminar flows. These are the Navier Stokes equations which comprise of formulae for the conservation of mass, momentum and energy:

Let the operator $$\nabla = i\frac{\partial}{\partial.x} + j\frac{\partial}{\partial.y} + k\frac{\partial}{\partial.z} = \left(\frac{\partial}{\partial.x}, \frac{\partial}{\partial.y}, \frac{\partial}{\partial.z}\right)$$

$$\frac{\partial.\rho}{\partial.t} = -\left[\frac{\rho.u}{\partial.x} + \frac{\rho.v}{\partial.y} + \frac{\rho.w}{\partial.z}\right]$$

$$\therefore \quad \frac{\partial.\rho}{\partial.t} + \nabla.(\rho.U) = 0$$

and $$\frac{\partial.\rho.U}{\partial.t} + \nabla.(\rho.U \otimes U) = B + \nabla\sigma$$

and $$\frac{\partial.\rho.H}{\partial.t} + \nabla.(\rho.UH) - \nabla.(\lambda.\nabla.T) = \frac{\partial.p}{\partial.t}$$

In addition there is a relationship between the stress and rate of strain, and two algebraic equations of state relating density to temperature and pressure, and one relating static enthalpy to temperature and pressure:

$$\sigma = -\rho.\delta + \mu.\left(\nabla.U + (\nabla.U)^T\right)$$

$$\rho = \rho_{(T,p)} \qquad h = h_{(T,p)} \qquad H = h + \frac{1}{2}U^2$$

The seven equations above plus boundary and initial conditions define the seven unknown functions, ρ, u, v, w, p, h, T.

If the flow is incompressible and μ is a constant, the number of equations can be reduced to four involving four unknown functions, u, v, w, p.

$$\frac{\partial \rho U}{\partial .t} + \nabla\left(\rho U \otimes U - \mu \nabla U\right) = B - \nabla p$$
$$\nabla U = 0$$

The equations for laminar flow are valid for turbulent flow aswell. However, we are limited in solving these equations accurately for high Reynolds numbers and we have to resort to turbulence modelling.

$$\text{Reynolds number } R_n = \frac{\rho.Ux}{\mu} = \frac{Ux}{\upsilon}$$

$$\text{where } \upsilon = \frac{\mu}{\rho} = \text{ kinematic viscosity } \left(m^2/s\right).$$

Reynolds-averaged Navier Sokes equations [11]

All the above transport equations can be expressed as a scalar advection-diffusion equation:

$$\frac{\partial .\rho .\Phi}{\partial .t} + \nabla .\left(\rho .U.\Phi - \Gamma .\nabla .\Phi\right) = S$$

where Γ = Diffusion coefficient.
Φ = A function of either mass, momentum, or heat.
S = Source or sink term representing the creation or destruction of Φ.

This equation is called the generic equation. For an example, take the case of the momentum in the y direction. The generic form of the equation can be written as:

$$\frac{\partial .\rho .V}{\partial .t} + \nabla .\left(\rho .U.V - \mu .\nabla .V\right) = B_y - \frac{\partial .p}{\partial .y}$$

Turbulent flows are extremely complex time-dependent flows governed by the laminar flow equations (Ref. 9). Applying Reynolds time averaging to the continuity equation (Ref. 9), the momentum equation and the scalar equation for incompressible flow, we obtain:

$$\frac{\partial .\rho}{\partial .t} + \nabla .\left(\rho .U\right) = 0$$
$$\frac{\partial .\rho .U}{\partial .t} + \nabla .\left(\rho .U \otimes U\right) = B + \nabla .\left(\sigma - \rho .\overline{u \otimes u}\right)$$

$$\frac{\partial.\rho.\Phi}{\partial.t} + \nabla.(\rho.U.\Phi) = \nabla.\left(\Gamma\nabla\Phi - \rho.\overline{u.\phi}\right) + S$$

The momentum and scalar transport equations contain additional terms. These are:

Reynolds Stress = $\rho.\overline{u \otimes u}$

Reynolds Flux = $\rho.\overline{u\phi}$

These terms arise from the non-linear corrective term in the unaveraged equations.

In addition to the above equations, complex eddy viscosity models are also used to express the Reynolds stress and Reynolds fluxes in terms of the mean quantities.

The default turbulent model in Flow3d is the $k-\varepsilon$ model and there are three versions available:

- The standard $k-\varepsilon$ model.
- The low Reynolds number $k-\varepsilon$ model - a modification of the standard $k-\varepsilon$ model to allow calculation of turbulent flows at low Reynolds numbers, typically in the range 5000 to 30,000.
- The RNG $k-\varepsilon$ model - an alternative to the standard $k-\varepsilon$ model for high Reynolds number flows. It has a modification to the equation for ε and uses a different set of model constraints [10,11].

Appendix B

CFX4.1-F3D Solution Strategy[10]

B1. DIFFERENCING SCHEMES

The numerical accuracy of the modelled equations to be solved to a large extent depend upon the method of discretization chosen for their advection terms. Various discretization methods are available in the software ranging from robust but relatively inaccurate hybrid and upwind schemes to more accurate but less robust higher order schemes. Hybrid differencing is the default scheme used to model the convective terms of all transport equations.

All equations except k and epsilon were left as hybrid schemes. The k and epsilon equations were set to use the CCCT scheme, a third order accurate method. Some higher order methods can suffer from non-physical overshoots, for example, turbulent kinetic energy could become negative. The CCCT method is bounded in order to eliminate these overshoots.

B2. VARIABLE ITERATIONS

To aid convergence it is sometimes necessary to alter the standard strategy by iterating on a subset of variables within each global iteration. This was done for the turbulence equations. Rather than the default one iteration, these were set to three iterations per global iteration. This did mean the solver required more CPU time but the solution will have been more accurate.

B3. UNDER-RELAXATION

Under-relaxation has several interlinked purposes in the solution process. Principally, the amount by which a variable would change if its discrete transport equation were solved as it stands is reduced. In this way difficulties caused by instability due, among other factors, to non-linearity are overcome. Under-relaxation for all the transport equations is implemented by scaling the coefficient of the variable in the current cell by an under-relaxation factor (URF) in the range $0<URF<1$. The smaller the factor, the more under-relaxation.

B4. DEFERRED CORRECTION

One of the most common causes of lack of convergence of turbulence flow calculations within CFX is due to the cross-derivative diffusion terms in the k and epsilon equations on non-orthogonal grids. There is a facility for under-relaxing these terms during the course of the calculation. A start iteration before which the terms are omitted and an end iteration after which the terms are included can be set. This was done for the first half of the total iterations carried out.

Appendix C

Tables of Results

Table C1: Velocity profiles through the duct at IVR=0.88.

Case 15-950
IVR = 0.88

Distance From Top Wall (mm)	Velocity (m/s)				
	Section EA	Section A	Section C	Section D	Section E
28	12.397	8.482	8.482	9.822	13.949
30	12.528	8.672	8.766	10.466	14.746
35	13.040	9.483	9.987	11.789	16.843
40	13.441	10.349	11.365	13.652	18.574
45	13.890	11.000	12.463	15.291	19.434
50	14.410	11.858	13.772	16.672	19.768
60	15.397	13.411	15.816	18.486	19.850
80	17.203	15.971	17.947	18.923	19.891
100	18.330	17.392	18.241	19.009	19.891
125	18.596	17.901	18.285	19.052	19.891
140	18.640	17.901	18.285	19.052	19.830
150	18.640	17.947	18.285	19.073	19.830
160	18.640	17.947	18.285	19.073	19.809
175	18.596	17.924	18.308	19.073	19.747
200	18.530	17.924	18.308	19.052	19.643
220	18.173	17.901	18.308	19.052	19.476
225	17.345	17.901	18.308	19.030	
230	15.660	17.901	18.308	19.009	19.308

Table C2: Velocity profiles through the duct at IVR=1.17.

Case 10-875
IVR = 1.17

Distance From Top Wall (mm)	Velocity (m/s)			
	Section EA	Section A	Section C	Section D
28	14.475	12.618	13.658	15.183
30	14.885	12.870	13.863	15.317
35	15.775	13.540	14.207	15.397
40	16.350	14.064	14.347	15.450
45	16.738	14.597	14.403	15.450
50	17.071	14.924	14.403	15.450
60	17.351	15.191	14.403	15.477
80	17.397	15.218	14.403	15.450
100	17.397	15.244	14.403	15.450
125	17.397	15.271	14.431	15.450
140	17.374	15.297	14.431	15.450
150	17.351	15.271	14.459	15.450
160	17.258	15.271	14.403	15.450
175	15.648	15.271	14.403	15.450
200	12.797	14.978	14.403	15.450
220	10.863	12.425	12.681	15.503
225		12.295	11.128	15.503
230		11.964	9.405	15.503

Table C3: Velocity profiles through the duct at IVR=1.41.

Case 10-1051
IVR = 1.41

Distance From Top Wall (mm)	Velocity (m/s)			
	Section EA	Section A	Section C	Section D
28	18.120	16.919	18.201	18.352
30	19.070	17.202	18.245	18.352
35	20.234	17.799	18.267	18.397
40	20.840	18.289	18.289	18.397
45	21.146	18.551	18.289	18.397
50	21.297	18.595	18.289	18.441
60	21.372	18.616	18.289	18.441
80	21.316	18.638	18.289	18.419
100	21.297	18.702	18.289	18.419
125	21.222	18.702	18.289	18.397
140	20.685	18.659	18.289	18.419
150	19.404	18.551	18.289	18.419
160	17.671	17.663	18.289	18.419
175	15.750	13.300	17.572	18.397
185			12.031	
200	15.126	10.572	-7.060	18.397
220	14.585	9.905	-7.390	16.425
225		10.066	-2.840	11.365
230		10.302	6.082	-8.290

Table C4: Experimental and CFD pressure coefficient distributions for three IVR's.

Top Centre-line

	Experiments			CFD		
X	Case 15-950 IVR = 0.88 Cp	Case 10-875 IVR = 1.17 Cp	Case 10-1051 IVR = 1.41 Cp	Case 15-950 IVR = 0.88 Cp	Case 10-875 IVR = 1.17 Cp	Case 10-1051 IVR = 1.41 Cp
-0.400				-0.053	-0.062	-0.077
-0.300	0.000	0.000	0.000	0.000	0.000	0.000
-0.250						
-0.200				0.128	0.146	0.180
-0.150	0.094	0.167	0.203			
-0.100				0.229	0.271	0.338
-0.030	0.029	0.184	0.204			
0.000				0.267	0.330	0.414
0.020	0.053	0.137	0.169			
0.100				0.209	0.267	0.333
0.115	-0.029	0.208	0.203			
0.165	0.003	0.204	0.220			
0.200				0.173	0.238	0.304
0.260	-0.064	0.127	0.223			
0.300	-0.028	0.165	0.246	0.136	0.241	0.340
0.382	-0.179	0.184	0.268			
0.400				0.066	0.248	0.408
0.437	-0.237	0.122	0.318			
0.500				-0.037	0.240	0.465
0.525	-0.366	0.128	0.311			
0.573	-0.392	0.098	0.337			
0.600				-0.167	0.209	0.488
0.655	-0.550	0.015	0.288			
0.692	-0.674	-0.041	0.269			
0.700				-0.351	0.132	0.457
0.748	-1.021	-0.314	0.128			
0.765	-1.048	-0.252	0.134			
0.796	-1.044	-0.217	0.147	-1.441	-0.518	-0.050

Bottom Centre-line

	Experiments			CFD		
X	Case 15-950 IVR = 0.88 Cp	Case 10-875 IVR = 1.17 Cp	Case 10-1051 IVR = 1.41 Cp	Case 15-950 IVR = 0.88 Cp	Case 10-875 IVR = 1.17 Cp	Case 10-1051 IVR = 1.41 Cp
-0.400				-0.159	-0.138	-0.133
-0.300				-0.156	-0.145	-0.148
-0.250	-0.339	-0.280	-0.328			
-0.200				-0.304	-0.268	-0.266
-0.160	-0.588	-0.454	-0.436			
-0.100				-0.498	-0.398	-0.355
-0.095	-0.500	-0.380	-0.304			
0.000				-0.065	-0.020	0.030
0.005	-0.101	-0.011	-0.052			
0.095	0.027	0.003	-0.102			
0.100				0.119	0.125	0.136
0.200				-0.412	-0.137	-0.430

Table C5: CFD duct + flat plate Cp distributions for various inflow conditions.

Top Centre-line.

	Half Jet + Plate				Full Jet + Plate	
X	0 Degrees Cp	7 Degrees Pitch Cp	15 Degrees Pitch Cp	.-7 Degrees Pitch Cp	5 Degrees Yaw Cp	10 Degrees Yaw Cp
-0.400	-0.057	-0.068	-0.070	-0.025	0.126	0.136
-0.300	0.000	0.000	0.000	0.000	0.000	0.000
-0.250						
-0.200	0.164	0.169	0.174	0.185	0.107	0.108
-0.150						
-0.100	0.244	0.251	0.262	0.275	0.208	0.210
-0.030						
0.000	0.322	0.328	0.341	0.371	0.268	0.272
0.020						
0.100	0.267	0.274	0.286	0.300	0.200	0.200
0.115						
0.165						
0.200	0.217	0.219	0.222	0.247	0.142	0.138
0.260						
0.300	0.214	0.192	0.173	0.279	0.136	0.132
0.382						
0.400	0.215	0.155	0.100	0.340	0.138	0.136
0.437						
0.500	0.207	0.102	0.009	0.393	0.133	0.135
0.525						
0.573						
0.600	0.177	0.028	-0.104	0.420	0.103	0.109
0.655						
0.692						
0.700	0.125	-0.071	-0.243	0.421	0.044	0.052
0.748						
0.765						
0.796	-0.231	-0.586	-0.915	0.201	-0.348	-0.336

Bottom Centre-line.

	Half Jet + Plate				Full Jet + Plate	
X	0 Degrees Cp	7 Degrees Pitch Cp	15 Degrees Pitch Cp	.-7 Degrees Pitch Cp	5 Degrees Yaw Cp	10 Degrees Yaw Cp
-0.400	-0.160	-0.144	-0.149	-0.243	-0.667	-0.686
-0.300	-0.157	-0.152	-0.159	-0.210	-0.401	-0.420
-0.250						
-0.200	-0.318	-0.334	-0.341	-0.335	-0.551	-0.553
-0.160						
-0.100	-0.523	-0.561	-0.562	-0.482	-0.482	-0.471
-0.095						
0.000	-0.066	-0.063	-0.053	-0.065	-0.154	-0.157
0.005						
0.095						
0.100	0.111	0.139	0.163	0.082	0.021	0.015
0.200	0.307	0.400	0.434	0.201	0.177	0.152

Table C6: CFD duct + hull Cp distributions for various inflow conditions.

Top Centre-line.

X	0 Degrees Cp	7 Degrees Pitch Cp	5 Degrees Yaw Cp	0 Degrees IVR=1.25 Cp
-0.400	-0.055	-0.117	-0.065	-0.047
-0.300	0.000	0.000	0.000	0.000
-0.250				
-0.200	0.163	0.113	0.161	0.169
-0.150				
-0.100	0.271	0.147	0.264	0.283
-0.030				
0.000	0.318	0.129	0.307	0.333
0.020				
0.100	0.268	0.057	0.256	0.279
0.115				
0.165				
0.200	0.220	-0.048	0.203	0.231
0.260				
0.300	0.235	-0.153	0.201	0.256
0.382				
0.400	0.260	-0.286	0.202	0.298
0.437				
0.500	0.281	-0.518	0.201	0.335
0.525				
0.573				
0.600	0.290	-0.932	0.188	0.360
0.655				
0.692				
0.700	0.280	-1.314	0.163	0.361
0.748				
0.765				
0.796	0.190	-1.903	0.057	0.286

Bottom Centre-line.

X	0 Degrees Cp	7 Degrees Pitch Cp	5 Degrees Yaw Cp	0 Degrees IVR=1.25 Cp
-0.400	-0.144	0.042	-0.130	-0.161
-0.300	-0.149	-0.082	-0.151	-0.159
-0.250				
-0.200	-0.341	-0.413	-0.365	-0.340
-0.160				
-0.100	-0.469	-0.716	-0.517	-0.447
-0.095				
0.000	-0.045	-0.187	-0.058	-0.039
0.005				
0.095				
0.100	0.093	0.079	0.102	0.087
0.200	0.179	0.419	0.290	0.112

Table C7: CFD duct + flat plate axial velocity distributions at exit for various inflow conditions.

IVR = 1.17

Axial Velocities at 0.7R at exit plane (m/s)

Degrees From TDC	Half Jet + Plate				Full Jet + Plate	
	0 Degrees Va	7 Degrees Pitch Va	15 Degrees Pitch Va	-7 Degrees Pitch Va	5 Degrees Yaw Va	10 Degrees Yaw Va
0	18.692	18.663	18.535	18.721	15.858	15.838
15	18.698	18.681	18.574	18.716	15.864	15.830
30	18.792	18.904	18.986	18.729	16.104	15.943
45	18.580	18.766	18.981	18.469	15.803	15.599
60	18.763	18.909	19.032	18.717	16.484	16.297
75	18.783	18.764	18.746	18.935	17.012	16.851
90	18.674	18.433	18.374	19.164	17.994	17.864
105	18.276	17.922	18.012	19.150	19.300	19.230
120	17.832	17.602	17.850	18.877	19.944	19.958
135	17.467	17.445	17.748	18.292	19.898	19.930
150	17.784	18.075	18.116	17.631	20.487	20.374
165	17.966	18.496	18.255	16.459	20.802	20.441
180	17.717	18.369	18.162	16.189	20.702	20.275
195	17.966				21.171	20.523
210	17.784				21.450	20.888
225	17.467				20.753	21.306
240	17.832				20.430	21.205
255	18.276				19.558	20.209
270	18.674				18.232	18.615
285	18.783				17.322	17.470
300	18.763				16.907	16.952
315	18.580				16.386	16.409
330	18.792				16.446	16.426
345	18.698				15.983	16.007
360	18.692				15.858	15.838

Table C8: CFD duct + flat plate radial velocity distributions at exit for various inflow conditions.

IVR = 1.17

Radial Velocities at 0.7R at exit plane (m/s)

Degrees From TDC	Half Jet + Plate				Full Jet + Plate	
	0 Degrees Vr	7 Degrees Pitch Vr	15 Degrees Pitch Vr	.-7 Degrees Pitch Vr	5 Degrees Yaw Vr	10 Degrees Yaw Vr
0	0.313	0.254	0.112	0.229	-0.778	-0.897
15	0.353	0.295	0.161	0.283	-0.625	-0.657
30	0.485	0.472	0.376	0.372	-0.580	-0.673
45	0.352	0.391	0.388	0.204	-0.624	-0.713
60	0.523	0.540	0.493	0.408	-0.296	-0.350
75	0.589	0.531	0.397	0.557	0.226	0.226
90	0.380	0.190	0.021	0.551	0.744	0.809
105	-0.133	-0.382	-0.467	0.249	1.212	1.416
120	-0.439	-0.631	-0.611	-0.007	1.053	1.401
135	-0.418	-0.519	-0.457	-0.096	1.027	1.443
150	-0.849	-0.721	-0.552	-0.910	0.617	1.128
165	-1.342	-0.977	-0.623	-1.594	0.113	0.661
180	-1.064	-0.793	-0.505	-1.198	0.298	1.000
195	-1.342				-0.375	0.359
210	-0.849				-0.427	-0.443
225	-0.418				0.129	-0.324
240	-0.439				0.095	-0.136
255	-0.133				0.289	-0.020
270	0.380				0.175	-0.290
285	0.589				-0.005	-0.456
300	0.523				-0.282	-0.517
315	0.352				-0.473	-0.519
330	0.485				-0.459	-0.594
345	0.353				-0.655	-0.756
360	0.313				-0.778	-0.897

Table C9: CFD duct + flat plate angular velocity distributions at exit for various inflow conditions.

IVR = 1.17

Angular Velocities at 0.7R at exit plane (m/s)

Degrees From TDC	Half Jet + Plate				Full Jet + Plate	
	0 Degrees Vw	7 Degrees Pitch Vw	15 Degrees Pitch Vw	-7 Degrees Pitch Vw	5 Degrees Yaw Vw	10 Degrees Yaw Vw
0	0.000	0.000	0.000	0.000	0.587	1.002
15	0.153	0.126	0.139	0.265	0.855	1.291
30	0.479	0.349	0.274	0.777	1.721	2.146
45	0.978	0.753	0.600	1.442	2.677	3.077
60	0.947	0.675	0.491	1.539	3.216	3.675
75	0.959	0.610	0.402	1.733	3.771	4.286
90	0.914	0.516	0.327	1.820	4.401	4.990
105	1.028	0.655	0.483	1.850	4.484	5.126
120	1.380	1.014	0.793	2.107	4.210	4.860
135	1.724	1.336	1.028	2.378	4.144	4.813
150	0.906	0.630	0.446	1.385	2.796	3.665
165	0.317	0.174	0.110	0.618	1.670	2.681
180	0.000	0.000	0.000	0.000	1.679	2.694
195	-0.317				0.487	1.436
210	-0.906				-0.671	0.492
225	-1.724				-2.282	-0.904
240	-1.380				-2.617	-1.499
255	-1.028				-3.066	-2.329
270	-0.914				-3.076	-2.420
285	-0.959				-2.606	-1.872
300	-0.947				-2.172	-1.423
315	-0.978				-1.781	-1.148
330	-0.479				-0.830	-0.337
345	-0.153				0.004	0.412
360	0.000				0.587	1.002

Table C10: CFD duct + hull axial velocity distributions at exit for various inflow conditions.

IVR = 1.17

Axial Velocities at 0.7R at exit plane (m/s)

Degrees From TDC	0 Degrees Va	7 Degrees Pitch Va	5 Degrees Yaw Va	0 Degrees IVR=1.25 Va
0	18.405	19.645	18.391	19.669
15	18.428	19.833	18.409	19.690
30	18.620	20.477	18.594	19.871
45	18.278	19.398	18.327	19.538
60	18.548	19.451	18.702	19.842
75	18.670	18.876	18.830	20.013
90	18.745	17.171	18.763	20.221
105	18.491	15.937	18.461	20.081
120	18.003	15.758	17.957	19.602
135	17.578	16.445	17.432	19.096
150	17.586	19.729	17.302	18.695
165	17.132	20.904	17.345	17.672
180	17.100	20.967	17.401	17.603
195	17.152	20.947	17.822	17.678
210	17.606	20.052	18.562	18.710
225	17.600	17.644	18.032	19.121
240	18.021	16.751	18.036	19.623
255	18.497	15.545	17.947	20.090
270	18.739	14.556	18.013	20.216
285	18.646	14.448	18.089	19.989
300	18.517	14.830	18.027	19.812
315	18.250	15.359	17.833	19.510
330	18.608	17.256	18.497	19.858
345	18.425	18.694	18.429	19.688
360	18.405	19.645	18.391	19.669

Table C11: CFD duct + hull radial velocity distributions at exit for various inflow conditions.

IVR = 1.17

Radial Velocities at 0.7R at exit plane (m/s)

Degrees From TDC	0 Degrees Vr	7 Degrees Pitch Vr	5 Degrees Yaw Vr	0 Degrees IVR=1.25 Vr
0	0.315	1.584	0.256	0.264
15	0.358	1.526	0.437	0.309
30	0.524	1.764	0.466	0.465
45	0.316	1.158	0.283	0.256
60	0.467	1.097	0.511	0.425
75	0.546	0.642	0.634	0.553
90	0.409	-0.296	0.499	0.501
105	-0.047	-1.103	0.203	0.083
120	-0.454	-1.391	-0.120	-0.371
135	-0.468	-1.219	-0.084	-0.392
150	-1.007	-1.309	-0.639	-1.039
165	-1.553	-1.313	-0.995	-1.667
180	-1.481	-1.305	-0.716	-1.579
195	-1.536	-1.255	-1.171	-1.656
210	-0.988	-1.164	-1.431	-1.023
225	-0.452	-0.844	-0.911	-0.377
240	-0.442	-0.793	-0.908	-0.358
255	-0.042	-0.714	-0.727	0.087
270	0.403	-0.661	-0.257	0.493
285	0.535	-0.311	0.208	0.541
300	0.457	0.200	0.433	0.414
315	0.310	0.495	0.489	0.25
330	0.521	1.139	0.789	0.462
345	0.357	1.389	0.464	0.308
360	0.315	1.584	0.256	0.264

Table C12: CFD duct + hull angular velocity distributions at exit for various inflow conditions.

IVR = 1.17

Angular Velocities at 0.7R at exit plane (m/s)

Degrees From TDC	0 Degrees Vw	7 Degrees Pitch Vw	5 Degrees Yaw Vw	0 Degrees IVR=1.25 Vw
0	0.000	-0.435	0.923	0.000
15	0.130	-0.718	0.909	0.156
30	0.534	-0.461	1.258	0.598
45	1.140	0.115	1.738	1.240
60	1.043	-0.573	1.644	1.188
75	0.991	-1.172	1.563	1.188
90	0.962	-1.549	1.549	1.204
105	1.043	-1.048	1.697	1.277
120	1.368	-0.301	2.095	1.623
135	1.682	0.262	2.462	1.925
150	0.820	-0.044	1.913	0.968
165	0.299	-0.127	1.589	0.375
180	0.000	0.153	1.695	0.000
195	-0.289	0.164	1.388	-0.378
210	-0.822	0.119	1.014	-0.974
225	-1.685	-0.027	0.089	-1.931
240	-1.370	0.278	0.274	-1.626
255	-1.043	0.597	0.518	-1.275
270	-0.961	0.915	0.612	-1.203
285	-0.990	0.690	0.400	-1.187
300	-1.036	0.126	0.149	-1.181
315	-1.129	-0.776	-0.225	-1.228
330	-0.513	-0.656	0.403	-0.577
345	-0.109	-0.647	0.681	-0.134
360	0.000	-0.435	0.923	0.000

Table C13: CFD duct + working section Cp distribution for different cell numbers.

Top Centre-line.

X	36280 Cells Cp	44280 Cells Cp	55720 Cells Cp
-0.400	-0.055	-0.061	-0.058
-0.300	0.000	0.000	0.000
-0.250			
-0.200	0.169	0.178	0.186
-0.150			
-0.100	0.248	0.257	0.263
-0.030			
0.000	0.326	0.333	0.344
0.020			
0.100	0.267	0.268	0.274
0.115			
0.165			
0.200	0.218	0.219	0.221
0.260			
0.300	0.225	0.227	0.227
0.382			
0.400	0.242	0.243	0.243
0.437			
0.500	0.248	0.247	0.246
0.525			
0.573			
0.600	0.226	0.225	0.221
0.655			
0.692			
0.700	0.178	0.176	0.178
0.748			
0.765			
0.796	-0.202	-0.203	-0.260

Bottom Centre-line.

X	36280 Cells Cp	44280 Cells Cp	55720 Cells Cp
-0.400	-0.168	-0.157	-0.170
-0.300	-0.161	-0.158	-0.167
-0.250			
-0.200	-0.314	-0.327	-0.333
-0.160			
-0.100	-0.500	-0.525	-0.526
-0.095			
0.000	-0.062	-0.067	-0.069
0.005			
0.095			
0.100	0.100	0.096	0.097
0.200	0.232	0.240	0.239

Appendix D

List of Duct Section Points.

Points Defining Water-jet Duct Sections.

Section 1

X (m)	Y (m)	Z (m)
-0.4	0.1500	0.0000
-0.4	0.1507	0.0131
-0.4	0.1527	0.0260
-0.4	0.1561	0.0386
-0.4	0.1608	0.0508
-0.4	0.1667	0.0625
-0.4	0.1738	0.0735
-0.4	0.1821	0.0836
-0.4	0.1914	0.0929
-0.4	0.2015	0.1012
-0.4	0.2125	0.1083
-0.4	0.2242	0.1142
-0.4	0.2364	0.1189
-0.4	0.2490	0.1223
-0.4	0.2619	0.1243
-0.4	0.2750	0.1250
-0.4	0.2821	0.1229
-0.4	0.2983	0.1195
-0.4	0.3198	0.1133
-0.4	0.3428	0.1034
-0.4	0.3633	0.0883
-0.4	0.3784	0.0678
-0.4	0.3883	0.0448
-0.4	0.3945	0.0233
-0.4	0.3979	0.0071
-0.4	0.4000	0.0000

Section 2

X (m)	Y (m)	Z (m)
-0.3	0.1500	0.0000
-0.3	0.1507	0.0131
-0.3	0.1527	0.0260
-0.3	0.1561	0.0386
-0.3	0.1608	0.0508
-0.3	0.1667	0.0625
-0.3	0.1738	0.0735
-0.3	0.1821	0.0836
-0.3	0.1914	0.0929
-0.3	0.2015	0.1012
-0.3	0.2125	0.1083
-0.3	0.2242	0.1142
-0.3	0.2364	0.1189
-0.3	0.2490	0.1223
-0.3	0.2619	0.1243
-0.3	0.2750	0.1250
-0.3	0.2908	0.1233
-0.3	0.3089	0.1190
-0.3	0.3281	0.1180
-0.3	0.3467	0.1017
-0.3	0.3633	0.0883
-0.3	0.3767	0.0717
-0.3	0.3868	0.0531
-0.3	0.3940	0.0339
-0.3	0.3983	0.0158
-0.3	0.4000	0.0000

Section 3

X (m)	Y (m)	Z (m)
-0.2	0.1493	0.0000
-0.2	0.1500	0.0131
-0.2	0.1521	0.0260
-0.2	0.1555	0.0386
-0.2	0.1601	0.0508
-0.2	0.1661	0.0625
-0.2	0.1732	0.0735
-0.2	0.1814	0.0836
-0.2	0.1907	0.0929

Section 3 (continued)

X (m)	Y (m)	Z (m)
-0.2	0.2009	0.1012
-0.2	0.2119	0.1083
-0.2	0.2236	0.1142
-0.2	0.2358	0.1189
-0.2	0.2484	0.1223
-0.2	0.2614	0.1243
-0.2	0.2744	0.1250
-0.2	0.2937	0.1235
-0.2	0.3125	0.1190
-0.2	0.3305	0.1117
-0.2	0.3472	0.1018
-0.2	0.3621	0.0895
-0.2	0.3750	0.0748
-0.2	0.3854	0.0581
-0.2	0.3930	0.0399
-0.2	0.3976	0.0207
-0.2	0.3993	0.0010
-0.2	0.3994	0.0004
-0.2	0.3994	0.0000

Section 4

X (m)	Y (m)	Z (m)
-0.1	0.1351	0.0000
-0.1	0.1358	0.0131
-0.1	0.1380	0.0260
-0.1	0.1414	0.0386
-0.1	0.1462	0.0508
-0.1	0.1523	0.0625
-0.1	0.1597	0.0735
-0.1	0.1681	0.0836
-0.1	0.1776	0.0929
-0.1	0.1881	0.1012
-0.1	0.1886	0.1015
-0.1	0.1993	0.1083
-0.1	0.2113	0.1142
-0.1	0.2237	0.1189
-0.1	0.2366	0.1223
-0.1	0.2498	0.1243
-0.1	0.2631	0.1250
-0.1	0.2798	0.1242
-0.1	0.2965	0.1219
-0.1	0.3128	0.1179
-0.1	0.3285	0.1124
-0.1	0.3434	0.1052
-0.1	0.3602	0.0928
-0.1	0.3723	0.0773
-0.1	0.3805	0.0591
-0.1	0.3852	0.0388
-0.1	0.3869	0.0167
-0.1	0.3874	0.0134
-0.1	0.3878	0.0100
-0.1	0.3883	0.0067
-0.1	0.3887	0.0033
-0.1	0.3892	0.0000

Section 5

X (m)	Y (m)	Z (m)
0	0.0952	0.0000
0	0.0960	0.0131
0	0.0982	0.0260
0	0.1020	0.0386
0	0.1038	0.0434
0	0.1071	0.0508
0	0.1137	0.0625
0	0.1215	0.0735
0	0.1306	0.0836
0	0.1394	0.0917

Section 5 (continued)

X (m)	Y (m)	Z (m)
0	0.1409	0.0929
0	0.1521	0.1012
0	0.1642	0.1089
0	0.1771	0.1142
0	0.1905	0.1189
0	0.1976	0.1208
0	0.2045	0.1223
0	0.2186	0.1243
0	0.2329	0.1250
0	0.2485	0.1250
0	0.2640	0.1248
0	0.2794	0.1244
0	0.2947	0.1236
0	0.3099	0.1224
0	0.3315	0.1156
0	0.3378	0.1117
0	0.3461	0.1037
0	0.3550	0.0876
0	0.3597	0.0677
0	0.3613	0.0444
0	0.3619	0.0355
0	0.3625	0.0266
0	0.3632	0.0177
0	0.3638	0.0088
0	0.3644	0.0000

Section 6

X (m)	Y (m)	Z (m)
0.1	0.0486	0.0000
0.1	0.0494	0.0131
0.1	0.0516	0.0260
0.1	0.0553	0.0386
0.1	0.0563	0.0411
0.1	0.0605	0.0508
0.1	0.0670	0.0625
0.1	0.0687	0.0651
0.1	0.0749	0.0735
0.1	0.0840	0.0836
0.1	0.0852	0.0848
0.1	0.0942	0.0929
0.1	0.1055	0.1012
0.1	0.1078	0.1027
0.1	0.1176	0.1083
0.1	0.1304	0.1142
0.1	0.1370	0.1167
0.1	0.1439	0.1189
0.1	0.1579	0.1223
0.1	0.1721	0.1243
0.1	0.1743	0.1245
0.1	0.1865	0.1250
0.1	0.2076	0.1250
0.1	0.2152	0.1250
0.1	0.2267	0.1250
0.1	0.2446	0.1250
0.1	0.2616	0.1250
0.1	0.2747	0.1250
0.1	0.2779	0.1250
0.1	0.2976	0.1242
0.1	0.3114	0.1183
0.1	0.3198	0.1076
0.1	0.3240	0.0927
0.1	0.3251	0.0738
0.1	0.3251	0.0591
0.1	0.3251	0.0444
0.1	0.3251	0.0296
0.1	0.3251	0.0148
0.1	0.3251	0.0000

Points Defining Water-jet Duct Sections.

Section 7

X (m)	Y (m)	Z (m)
0.2	0.0000	0.0000
0.2	0.0027	0.0131
0.2	0.0050	0.0260
0.2	0.0083	0.0375
0.2	0.0087	0.0386
0.2	0.0139	0.0508
0.2	0.0178	0.0582
0.2	0.0204	0.0625
0.2	0.0283	0.0735
0.2	0.0285	0.0737
0.2	0.0374	0.0836
0.2	0.0404	0.0866
0.2	0.0476	0.0929
0.2	0.0538	0.0977
0.2	0.0588	0.1012
0.2	0.0691	0.1073
0.2	0.0709	0.1083
0.2	0.0838	0.1142
0.2	0.0870	0.1155
0.2	0.0973	0.1189
0.2	0.1084	0.1217
0.2	0.1112	0.1223
0.2	0.1255	0.1243
0.2	0.1348	0.1249
0.2	0.1399	0.1250
0.2	0.1630	0.1250
0.2	0.1670	0.1250
0.2	0.1908	0.1250
0.2	0.1953	0.1250
0.2	0.2123	0.1250
0.2	0.2322	0.1250
0.2	0.2359	0.1250
0.2	0.2510	0.1250
0.2	0.2620	0.1244
0.2	0.2702	0.1214
0.2	0.2759	0.1159
0.2	0.2793	0.1081
0.2	0.2810	0.0981
0.2	0.2810	0.0785
0.2	0.2810	0.0590
0.2	0.2810	0.0394
0.2	0.2810	0.0197
0.2	0.2810	0.0000

Section 8

X (m)	Y (m)	Z (m)
0.3	0.0000	0.0921
0.3	0.0010	0.0929
0.3	0.0112	0.1005
0.3	0.0122	0.1012
0.3	0.0237	0.1080
0.3	0.0243	0.1083
0.3	0.0372	0.1142
0.3	0.0375	0.1144
0.3	0.0507	0.1189
0.3	0.0529	0.1195
0.3	0.0646	0.1223
0.3	0.0703	0.1232
0.3	0.0789	0.1243
0.3	0.0904	0.1250
0.3	0.0933	0.1250
0.3	0.1177	0.1250
0.3	0.1207	0.1250
0.3	0.1458	0.1250
0.3	0.1482	0.1250
0.3	0.1740	0.1250
0.3	0.1756	0.1250

Section 8 (continued)

X (m)	Y (m)	Z (m)
0.3	0.2022	0.1250
0.3	0.2029	0.1250
0.3	0.2240	0.1250
0.3	0.2259	0.1242
0.3	0.2276	0.1231
0.3	0.2291	0.1218
0.3	0.2305	0.1203
0.3	0.2318	0.1186
0.3	0.2318	0.0949
0.3	0.2318	0.0712
0.3	0.2318	0.0475
0.3	0.2318	0.0237
0.3	0.2318	0.0000

Section 9

X (m)	Y (m)	Z (m)
0.4	0.0000	0.1176
0.4	0.0040	0.1189
0.4	0.0136	0.1214
0.4	0.0180	0.1223
0.4	0.0286	0.1239
0.4	0.0322	0.1243
0.4	0.0452	0.1250
0.4	0.0466	0.1250
0.4	0.0686	0.1250
0.4	0.0741	0.1250
0.4	0.1001	0.1250
0.4	0.1016	0.1250
0.4	0.1282	0.1250
0.4	0.1290	0.1250
0.4	0.1564	0.1250
0.4	0.1839	0.1250
0.4	0.1839	0.1146
0.4	0.1839	0.1048
0.4	0.1839	0.0946
0.4	0.1839	0.0845
0.4	0.1839	0.0744
0.4	0.1839	0.0595
0.4	0.1839	0.0446
0.4	0.1839	0.0298
0.4	0.1839	0.0149
0.4	0.1839	0.0000

Section 10

X (m)	Y (m)	Z (m)
0.5	0.0000	0.1250
0.5	0.0166	0.1250
0.5	0.0276	0.1250
0.5	0.0369	0.1250
0.5	0.0550	0.1250
0.5	0.0624	0.1250
0.5	0.0825	0.1250
0.5	0.0951	0.1250
0.5	0.1099	0.1250
0.5	0.1373	0.1250
0.5	0.1373	0.1000
0.5	0.1373	0.0750
0.5	0.1373	0.0500
0.5	0.1373	0.0250
0.5	0.1373	0.0000

Section 11

X (m)	Y (m)	Z (m)
0.6	0.0000	0.1250
0.6	0.0085	0.1250
0.6	0.0213	0.1250
0.6	0.0360	0.1250
0.6	0.0473	0.1250
0.6	0.0635	0.1250
0.6	0.0798	0.1250
0.6	0.0909	0.1250
0.6	0.0909	0.1000
0.6	0.0909	0.0750
0.6	0.0909	0.0500
0.6	0.0909	0.0250
0.6	0.0909	0.0000

Section 12

X (m)	Y (m)	Z (m)
0.7	0.0000	0.1250
0.7	0.0170	0.1250
0.7	0.0259	0.1250
0.7	0.0445	0.1250
0.7	0.0445	0.1000
0.7	0.0445	0.0750
0.7	0.0445	0.0500
0.7	0.0445	0.0250
0.7	0.0445	0.0000

Section 13

X (m)	Y (m)	Z (m)
0.796	0.0000	0.1250
0.796	0.0000	0.1000
0.796	0.0000	0.0000